Journal of Cleaner Production 318 (2021) 128606

Contents lists available at ScienceDirect

Journal of Cleaner Production

journal homepage: www.elsevier.com/locate/jclepro

Sustainability assessment of biomethanol production via hydrothermal gasification supported by artificial neural network

Dániel Fózer [a,b,*], András József Tóth [a], Petar Sabev Varbanov [c], Jiří Jaromír Klemeš [c], Péter Mizsey [d]

[a] Department of Chemical and Environmental Process Engineering, Budapest University of Technology and Economics, Budafoki út 8, 1111, Budapest, Hungary
[b] Division for Sustainability, Department of Technology, Management and Economics, Technical University of Denmark, Produktionstorvet, Building, 424, DK-2800 Kgs. Lyngby, Denmark
[c] Sustainable Process Integration Laboratory – SPIL, NETME Centre, FME, Brno University of Technology– VUT Brno, Technická 2896/2, 616 69, Brno, Czech Republic
[d] Department of Fine Chemicals and Environmental Technology, University of Miskolc, Egyetem út, 3515, Miskolc, Hungary

ARTICLE INFO

Handling editor: Cecilia Maria Villas Bôas de Almeida

Keywords:
Biomethanol
Hydrothermal gasification
Artificial neural networks
Life cycle assessment
Cost analysis
Power-to-Liquid

ABSTRACT

Global warming and climate change urge the deployment of close carbon-neutral technologies via the synthesis of low-carbon emission fuels and materials. An efficient intermediate product of such technologies is the biomethanol produced from biomass. Microalgae based technologies offer scalable solutions for the biofixation of CO_2, where the produced biomass can be transformed into value-added fuel gas mixtures by applying thermochemical processes. In this study, the environmental and economic performances of biomethanol production are examined using artificial neural networks (ANNs) for the modelling of catalytic and noncatalytic hydrothermal gasification (HTG). Levenberg-Marquardt and Bayesian Regularisation algorithms are applied to describe the thermocatalytic transformation involving various types of feedstocks (biomass and wastes) in the training process. The relationship between the elemental composition of the feedstock, HTG reaction conditions (380 °C–717 °C, 22.5 MPa–34.4 MPa, 1–30 wt% biomass-to-water ratio, 0.3 min–60.0 min residence time, up to 5.5 wt% NaOH catalyst load) and fuel gas yield & composition are determined for *Chlorella vulgaris* strain. The ideal ANN topology is characterised by high training performance (MSE = 5.680E-01) and accuracies ($R^2 \geq 0.965$) using 2 hidden layers with 17-17 neurons. The process flowsheeting of biomass-to-methanol valorisation is performed using ASPEN Plus software involving the ANN-based HTG fuel gas profiles. Cradle-to-gate life cycle assessment (LCA) is carried out to evaluate the climate change potential of biomethanol production alternatives. It is obtained that high greenhouse gas (GHG) emission reduction (-725 kg $CO_{2,eq}$ (t $CH_3OH)^{-1}$) can be achieved by enriching the HTG syngas composition with H_2 using variable renewable electricity sources. The utilisation of hydrothermal gasification for the synthesis of biomethanol is found to be a favourable process alternative due to the (*i*) variable synthesis gas composition, (*ii*) heat integration, and (*iii*) GHG emission mitigation possibilities.

1. Introduction

The sustainable transformation and development of our society into a close zero-waste economy necessitate a whole-scale transition towards carbon emissions neutrality (Kerdlap et al., 2019). Drawing the directions of future-proof environmental technologies and the real advancement of chemical processes demand the minimisation of environmental footprints, as greenhouse gas (GHG) (Čuček et al., 2012), Nitrogen Footprint (Čuček et al., 2011) and also the other emissions footprints (Klemeš et al., 2020). The utilisation and deployment of variable renewable energy (VRE) sources (e.g., wind turbines and photovoltaic panels) have a determinant role in achieving ambitious climate goals and increasing the independence from conventional petrochemical materials (Deng and Lv, 2020). Harvesting the environmental benefits of clean fluctuating energy requires to (i) improve long-term and large-scale storage of intermittent renewable electricity (Liebensteiner and Wrienz, 2020), (ii) advance CO_2 capture and recycling technologies (Song et al., 2019), and (iii) design robust and feasible

* Corresponding author. Department of Chemical and Environmental Process Engineering, Budapest University of Technology and Economics, Budafoki út 8, 1111, Budapest, Hungary.
E-mail addresses: danfo@dtu.dk, daniel.fozer@edu.bme.hu (D. Fózer).

https://doi.org/10.1016/j.jclepro.2021.128606
Received 9 January 2021; Received in revised form 28 July 2021; Accepted 9 August 2021
Available online 12 August 2021

Power-to-X processes (Wu et al., 2021a).

Methanol, as a platform molecule, plays an important role in the framework of the circular economy (Fan et al., 2019), and it offers a wide variety of advantages (Olah, 2005). Methanol is a promising Power-to-Liquid (P2L) target compound that meets transportation, safety and infrastructure availability requirements (Zhang and Desideri, 2020). The storage of surplus variable renewable energy and decarbonisation of the chemical industry are unsolved challenges where sustainable methanol synthesis could have a high impact in the future. The conventional synthesis of methanol is based on the catalytic conversion of synthesis gas that is produced by the reforming of fossil resources (e.g., natural gas, coal) (Blumberg et al., 2019). Biomass-to-methanol (BTM) alternatives are gaining high interests due to the GHG emission reduction potentials over conventional technologies. Qin et al. (2021) discussed that applying coal-based methanol production with biomass co-gasification is a favourable technological pairing to decrease greenhouse gas emissions. It was also pointed out that the energy conversion efficiency of the BTM technology is lower compared to conventional alternatives. Hennig and Haase (2021) showed that a hydrogen enhanced BTM process could be operated at higher carbon and energy efficiencies compared to an unmodified BTM baseline scenario. However, it was highlighted that using alkaline electrolysis in the process makes biomethanol production highly unprofitable. These findings call attention to develop the technological readiness of bioenergy-based methanol production, including profitability (Butera et al., 2021), energy efficiency (Liu et al., 2021) and environmental aspects (Wu et al., 2021b). For these reasons, *ex-ante* synthesis and screening of promising Bioenergy with Carbon Capture and Utilisation (BECCU) process layouts are needed to support the development of robust and close-carbon neutral technologies.

The transformation of high moisture containing biomass to synthetic materials is a challenging task from the thermochemical point of view. Atmospheric conversion technologies require input raw materials with low moisture content (<5 wt%), which makes necessary the utilisation of high energy-consuming drying steps. Hydrothermal gasification (HTG) gained close attention because wet organic and inorganic feedstocks (biomass (Macrì et al., 2020), waste (Su et al., 2020), plastics (Bai et al., 2020)) can be converted in a process into value-added products. Fuel gas composition can be influenced by process parameters (temperature, pressure, feedstock-to-water ratio), homogeneous (Adar et al., 2020) and heterogeneous (Abdpour and Santos, 2021) catalysts. The high flexibility and in-process controllability of hydrothermal conversion can be used to improve waste and biomass valorisation pathways, including renewable hydrogen production (Chen et al., 2019b) or Power-to-Gas applications (Fózer et al., 2020). In order to analyse biomass-to-methanol upgrading via HTG, a detailed and accurate model-based representation of supercritical water gasification is required. Yukananto et al. (2018) developed a computational fluid dynamic model for the supercritical water gasification (SCWG) of glycerol, where the highest error of the model was 16%. Authors dos Santos and Pereira (2021) used a thermodynamic mathematic model to describe the gasification of liquid biomass in supercritical water. Okolie et al. (2020) developed a statistical model using response surface methodology to model the hydrothermal gasification of cellulose, hemicellulose and lignin. However, the accurate and detailed investigation of hydrothermal gasification (including optimisation, examining the main and interacting effects of independent process variables) and the synthesis of low-carbon emission chemicals using hydrothermal technology are limited by the lack of available descriptive HTG models. The limitations of available models are that (i) they involve only the investigation of a few specific model feedstocks, (ii) the independent variables and experimental conditions are examined in narrow intervals, (iii) reactor specifications are not considered directly and (iv) the error of models can be high.

The accurate modelling of biomass decomposition at high temperature and pressure conditions is a complicated task due to the high number of parallel occurring reactions, e.g., hydrolysis, decomposition, hydrogenation, deamination, decarboxylation, C-C breaking, dealkylation, hydroxylation, etc. (Wei et al., 2021). The benefit of machine learning is the ability to make fast and accurate predictions for non-linear computational tasks compared to already available techniques (such as density functional theory) (Csányi et al., 2020). The utilisation of artificial neural networks (ANN) - a sub-discipline of machine learning - is already demonstrated in chemical (Tai et al., 2020) and environmental-related (Poznyak et al., 2019) applications. The ANN was inspired by the biological neural network that can be used to describe complex and/or non-linear relationships. The application of neural networks has been discussed in the field of thermochemical conversions, including the co-pyrolysis of rice husk and sewage sludge (Naqvi et al., 2019), atmospheric biomass gasification (Cerinski et al., 2020), waste tyre blends (Ozonoh et al., 2020) and organic food waste (Gonçalves Neto et al., 2021).

The life cycle assessment (LCA) of methanol production have been performed analysing the environmental performance of various process configurations (Gautam et al., 2020) and feedstocks (e.g., wood (Yadav et al., 2020), rice straw (Im-orb and Arpornwichanop, 2020), coal (Liu et al., 2020) and natural gas (Li et al., 2018)). The GHG footprint of conventional methanol production is considered to be high ranging between 0.54 (Pérez-Fortes et al., 2016) and 3.56 kg $CO_{2,eq}$ (kg MeOH)$^{-1}$ (Qin et al., 2016). The involvement of renewable sources was found to be beneficial to decrease the environmental damages of methanol synthesis. Chen et al. (2019c) performed an LCA on an integrated atmospheric biomass gasification cycle and obtained negative GHG emission (−109.2 kg $CO_{2,eq}$ (kg MeOH)$^{-1}$). Adnan and Kibria (2020) concluded that Power-to-Methanol pathways offer climate benefits with negative carbon emission values (ranging from −325 to −654 kg $CO_{2,eq}$ (kg MeOH)$^{-1}$) using variable renewable solar energy for the conversion. Atmospheric thermochemical valorisation processes and methanol synthesis routes are already demonstrated in the literature as it is discussed above but there is a lack of knowledge considering the environmental impacts and viability of hydrothermal conversion based biomethanol production.

This work investigates the sustainability of a novel biomethanol production alternative using hydrothermal gasification in the process chain. Multiscale computational simulations are carried out incorporating machine learning, process flowsheeting and life cycle and cost analyses. Artificial neural networks are constructed and applied for the simulation of catalytic and noncatalytic thermochemical conversions of various biomass and waste feedstocks. A valorisation pathway for high moisture containing microalgae biomass is proposed involving the integration of fluctuating renewable energy. The environmental performance and GHG footprint of *in-situ* and external renewable H_2 generation strategies are investigated. It is obtained that the hydrothermal gasification-based biomass-to-methanol upgrading is characterised by low climate change impacts and enhanced decarbonisation properties compared to conventional technologies.

2. Novel approach and updated methods

The flowchart of the computational framework and simulation methodology is presented in Fig. 1. The missing elements of life cycle inventory (composition and properties of streams, thermochemical performance, reaction characteristics, heat integration possibilities) were determined by conducting process modelling and synthesis that had been supported by supervised machine learning. The flowsheeting was performed by ASPEN Plus v11 software (AspenTech, 2020). The thermodynamic properties were calculated by the Predictive Soave–Redlich–Kwong (PSRK) equation of the state method. The biomethanol production stages, boundaries and limitations are described in Section 2.1.

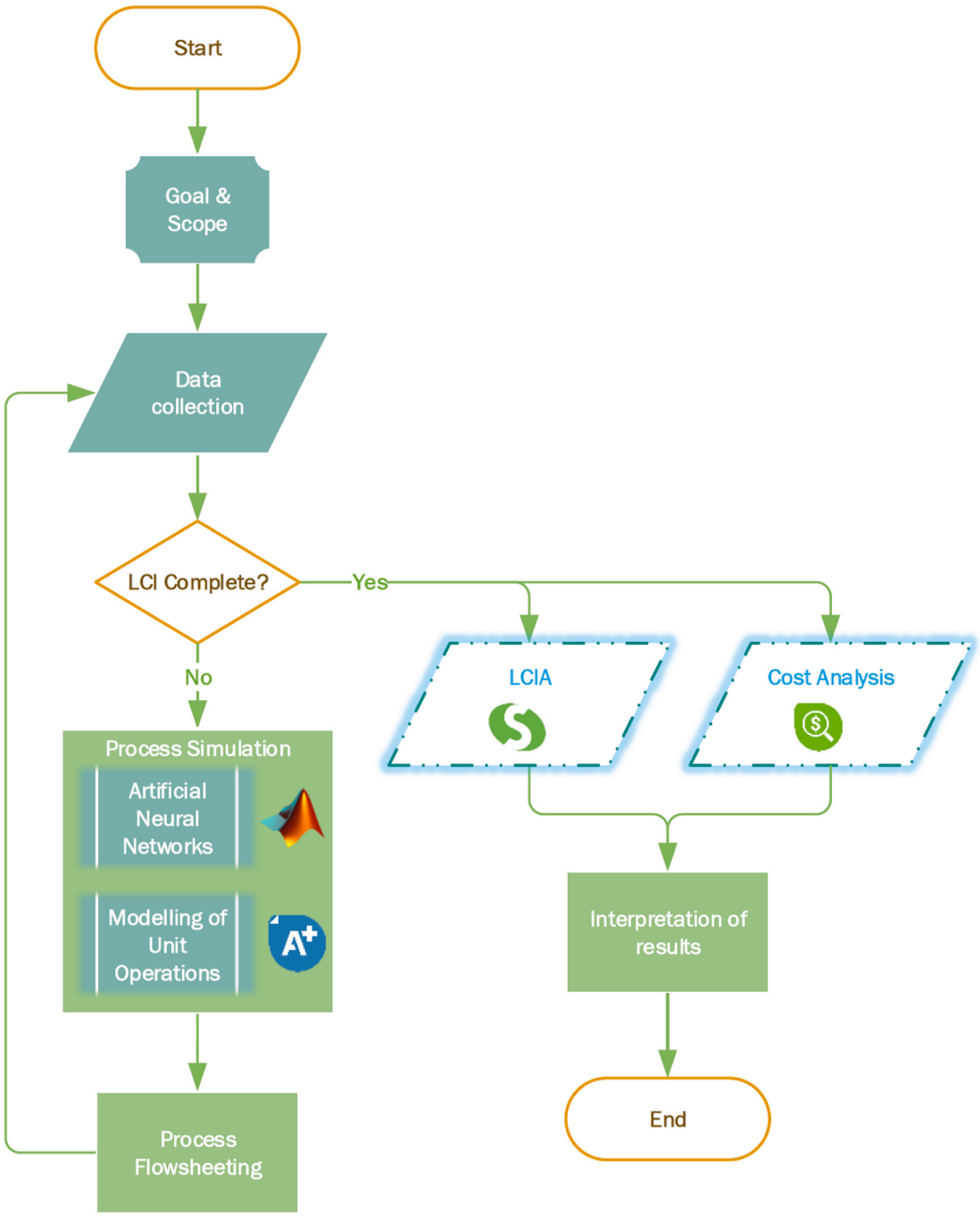

Fig. 1. Flowchart of the overall methodology. LCI: Life Cycle Inventory, LCIA: Life Cycle Impact Assessment.

2.1. Technology overview

2.1.1. Water electrolysis

Water electrolysis – as the cornerstone of Power-to-X applications – is a disruptive technology regarding the energy industry. The most advanced methods are alkaline electrolysis (AEL), Polymer Electrolyte Membrane (PEM) and Solid Oxide electrolysis (SOEL). The specific energy consumption of these technologies ranges between 3.7 and 6.5 kWh $(Nm^3\ H_2)^{-1}$ (Buttler and Spliethoff, 2018). For consisting of the energy balance of biomethanol production, the alkaline type electrolyser was considered in the calculations with an average energy consumption of 4.6 kWh $(Nm^3\ H_2)^{-1}$.

2.1.2. Biological CO_2 capture

CO_2 removal can be carried out by physical (adsorption), chemical (absorption) and biological ways (photosynthetic or hydrogenotrophic organisms) (Bhatia et al., 2019). Microalgae biomass has (i) outstanding photosynthetic activity compared to terrestrial crops, (ii) excellent biomass productivity and (iii) it can capture carbon dioxide directly from various sources (air, industrial flue gas) (Dvoretsky et al., 2020). *Chlorella vulgaris* algae strain was considered for the capture of CO_2. The aquatic biomass was defined as a non-conventional solid material based on its elemental and proximate compositions as follow (Belotti et al., 2014): C: 41.1 wt%; H: 6.4 wt%; N: 7.3 wt%; O: 40.5 wt%; S: 0 wt%; VM: 73.4 wt%; FC: 21.9 wt%; Ash: 4.7 wt%.

It was estimated that the biomass had been cultivated in open raceway ponds equipped with paddlewheels. Ammonium nitrate and

ammonium nitrate phosphate fertilisers were considered as N and P substrates. Following the cultivation phase, the biomass suspension was pre-concentrated using flocculation and centrifugation and transferred to the thermochemical plant via pipelines.

2.1.3. Thermochemical valorisation of biomass

Hydrothermal gasification was considered for the conversion of high moisture containing aquatic biomass. The gaseous product – HTG fuel gas – contains mainly H_2, CH_4, CO_2, CO and C_{2+} compounds. The application of a homogeneous catalyst (i.e., sodium hydroxide alkali metal) was investigated in the process chain to improve the conversion of the feedstock, influence the composition of the gas phase and increase H_2 and total gas yields (Kumar et al., 2018). A descriptive artificial neural network was developed for the modelling of hydrothermal conversion, as is detailed in Section 2.3. The designed neural network was used to calculate the product stream properties (fuel gas yield and composition) of the HTG operational unit and to provide data to the flowsheeting simulation stage. The total gas yield (Y_{GAS} (mol kg^{-1}) and carbon conversion ratio (CCR (%)) were determined by Eqs. (1) and (2):

$$Y_{GAS}\left(mol\ kg^{-1}\right) = \sum Y_{GAS,i} \quad i = H_2,\ CH_4,\ CO_2,\ CO, C_2H_4, C_2H_6 \tag{1}$$

$$CCR\ (\%) = \frac{\sum\left(m_{GAS,j}\cdot\frac{MW_C}{MW_{GAS,j}}\right)}{m_{feedstock}\cdot\frac{w_{C,feedstock}}{MW_C}} \quad j = CH_4,\ CO_2,\ CO, C_2H_4, C_2H_6 \tag{2}$$

where $Y_{GAS,i}$ (mol kg^{-1}) is the yield of the ith gas component, $m_{GAS,j}$ and $m_{feedstock}$ are the weight of the jth gas component and the feedstock (kg), MW_C and $MW_{GAS,j}$ are the molar weights of carbon, and the jth gas component (kg $kmol^{-1}$), $w_{C,feedstock}$ is the carbon content of the feedstock (wt.%).

2.1.4. HTG fuel gas reforming

Fuel gas reforming was simulated to produce high-quality synthesis gas for methanol synthesis. The biogas upgrading was carried out in two stages. First, pre-reforming was considered for the transformation of C_{2+} compounds (Eq. (3)) into a mixture of hydrogen and carbon monoxide. In the second step, tri-reforming of methane was taken place that is the combination of (*i*) partial oxidation (POX) (Eq. (4)), (*ii*) steam reforming (SRM) (Eq. (5)) and (*iii*) dry reforming (DRM) (Eq. (6)) reactions.

$$C_nH_m + nH_2O \leftrightarrow nCO + \frac{m+2n}{2}H_2 \tag{3}$$

$$CH_4 + \frac{1}{2}O_2 \rightarrow CO + 2H_2 \tag{4}$$

$$CH_4 + H_2O \leftrightarrow CO + 3H_2 \tag{5}$$

$$CH_4 + CO_2 \leftrightarrow 2CO + 2H_2 \tag{6}$$

2.1.5. Methanol synthesis

Synthesis gas is a versatile feedstock that can be used to produce a wide range of chemical products (e.g., alcohols, hydrocarbons and ethers). CO, CO_2 hydrogenations, and reverse water gas shift reaction (RWGSR) (Eqs. (7)–(9)) were considered for the synthesis of biomethanol. The syngas composition has an important role in achieving high methanol concentration in the product stream. Lerner et al. (2018) reported that a syngas modular of 2 is required to maximise the achievable methanol yield in the process. The synthesis gas modular (M_{SG}, Eq. (10)) was adjusted to reach the ideal level of methanol synthesis by using renewable hydrogen from external sources.

$$CO + 2H_2 \leftrightarrow CH_3OH \tag{7}$$

$$CO_2 + 3H_2 \leftrightarrow CH_3OH + H_2O \tag{8}$$

$$CO_2 + H_2 \leftrightarrow CO + H_2O \tag{9}$$

$$M_{SG}\ (-) = \frac{Z_{H_2} - Z_{CO_2}}{Z_{CO} + Z_{CO_2}} \tag{10}$$

Langmuir-Hinshelwood-Hougen-Watson (LHHW) kinetics was applied for the simulation of MeOH production. The rate equations, kinetic factors, constants for driving force and adsorption terms are given in Equations (11)–(13) and Tables 1–3 (Kiss et al., 2016):

$$r_A = k_A \frac{K_{CO}\left[f_{CO}f_{H_2}^{1.5} - \frac{f_{CH_3OH}}{\left(K_A f_{H_2}^{0.5}\right)}\right]}{\left(1 + K_{CO}f_{CO} + K_{CO_2}f_{CO_2}\right)\left[f_{H_2}^{0.5} + \left(\frac{K_{H_2O}}{K_H^{0.5}}\right)f_{H_2O}\right]} \tag{11}$$

$$r_B = k_B \frac{K_{CO_2}\left[f_{CO_2}f_{H_2}^{1.5} - \frac{f_{H_2O}f_{CH_3OH}}{\left(f_{H_2}^{1.5}K_B\right)}\right]}{\left(1 + K_{CO}f_{CO} + K_{CO_2}f_{CO_2}\right)\left[f_{H_2}^{0.5} + \left(\frac{K_{H_2O}}{K_H^{0.5}}\right)f_{H_2O}\right]} \tag{12}$$

$$r_C = k_C \frac{K_{CO_2}\left[f_{CO_2}f_{H_2} - \frac{f_{H_2O}f_{CO}}{K_C}\right]}{\left(1 + K_{CO}f_{CO} + K_{CO_2}f_{CO_2}\right)\left[f_{H_2}^{0.5} + \left(\frac{K_{H_2O}}{K_H^{0.5}}\right)f_{H_2O}\right]} \tag{13}$$

where f_k is the fugacity of components (Pa), k_A, k_B, k_C are kinetic factors. K_A (Pa^{-2}), K_B (Pa^{-2}), K_C (−) are the equilibrium constants of reactions, K_k is the adsorption equilibrium constant of component k (Pa^{-1}), where k equals to H_2, H_2O, CO, CO_2.

2.2. Environmental evaluation

The environmental screening of biomethanol production was evaluated by performing a cradle-to-gate life cycle assessment (LCA) according to ISO 14040 and 14044 standards. SimaPro 9.1.1.1 software (PRé Sustainability, 2020) was used to perform LCAs where the life cycle inventory was compiled based on (i) the Ecoinvent v3.4 database, (ii) literature data, (iii) ASPEN Plus v11 and (iv) MATLAB R2020a (MathWorks, 2020) simulation results. The life cycle inventory is summarised in Table 4. Life cycle impact assessment was carried out using the IMPACT2002+ v2.14 method. The investigated cradle-to-gate life cycle system boundary, the operational units, utilities and additional elements are illustrated in Fig. 2. The functional unit of LCA was 1 t of produced biomethanol.

2.3. Cost estimation

Economic analysis is conducted to estimate the costs of the HTG-based biomethanol production plant. The Marshall and Swift (M&S) indexation method and ASPEN Process Economic Analyzer v11 (APEA, 2021) software tool were used to determine the cost of equipment. Cost functions and parameters are summarised in Table 5. The total annual cost (TAC) was calculated by Eq. (14):

$$TAC\ \left(€\ y^{-1}\right) = C_{OPEX} + C_{CAPEX} \tag{14}$$

where C_{OPEX} is the operation expenditure (€ y^{-1}), C_{CAPEX} is the

Table 1
LHHW kinetic factors for reaction rate expressions (Eqs. (11)–(13)). k is the pre-exponential factor, E_a is the activation energy.

Reaction	k	E_a (J mol^{-1})
A	4.0638E-06 (kmol (kg_{cat} s Pa)$^{-1}$)	11,695
B	1.5188E-33 (kmol (kg_{cat} s Pa)$^{-1}$)	266,010
C	9.0421E+08 (kmol (kg_{cat} s $Pa^{0.5}$)$^{-1}$)	112,860

Table 2
Driving force constants of methanol synthesis. In Aspen Plus simulations, the driving force is expressed in K_1 and K_2 generalised forms for forward and reverse cases.

Reaction	K_1 (forward)	K_2 (reverse)
A	8.3965E-11 exp(118,270(RT)$^{-1}$) (Pa^{-1})	3.5408E+12 exp(19,832(RT)$^{-1}$) (Pa)
B	1.7214E-10 exp(81,287(RT)$^{-1}$) (Pa^{-1})	2.5813E+10 exp(26,788(RT)$^{-1}$) (Pa)
C	1.7214E-10 exp(81,287(RT)$^{-1}$) (Pa^{-1})	6.1221E-13 exp(125,226(RT)$^{-1}$) (Pa)$-^{1}$

Table 3
LHHW adsorption equilibrium constants and terms for methanol synthesis. $K_i = a_i exp(b_i(RT)^{-1})$.

Adsorption term	Expressed form	Pre-exponential factor (a_i)	$A_i = \ln a_i$	b_i (J mol^{-1})	$B_i = b_i R^{-1}$
1	1	1	0	0	0
2	$\frac{K_{H_2O}}{K_H^{0.5}}$	4.3686E-12 ($Pa^{-0.5}$)	−26.1568	1.1508E+05	13,842
3	K_{CO}	8.3965E-11 (Pa^{-1})	−23.2006	1.1827E+05	14,225
4	$\frac{K_{CO}K_{H_2O}}{K_H^{0.5}}$	3.6673E-22 ($Pa^{-1.5}$)	−49.3574	2.3335E+05	28,067
5	K_{CO_2}	1.7214E-10 (Pa^{-1})	−22.4827	8.1287E+04	9,777
6	$\frac{K_{CO_2}K_{H_2O}}{K_H^{0.5}}$	7.5184E-22 ($Pa^{-1.5}$)	48.6395	1.9637E+05	23,619

annualised capital expenditure (€ y^{-1}) defined by Eq. (15):

$$C_{CAPEX}\left(€\ y^{-1}\right) = CRF \cdot TPC \tag{15}$$

where CRF is the capital recovery factor (−), TPC is the total plant cost (€). CRF was determined based on Eq. (16):

$$CRF = \frac{R_i(1+R_i)^N}{(1+R_i)^N - 1} \tag{16}$$

The plant lifetime (N) and rate of interest (R_i) were assumed to be 25 years and 5%.

2.4. Artificial neural network (ANN)

ANN had a long period of intensive development (Klemeš and Ponton, 1992) and also various alternatives were developed (Ponton and Klemeš, 1993). After an assessment Feed-forward backpropagation (FFBP) machine learning algorithm was applied for the modelling of biomass hydrothermal conversion. A Multilayer Perceptron (MLP) consists of input, output and hidden layers. The input layer takes in input data (independent variables), and the output layer provides computed target values (dependent variables). The computational process is carried out in the hidden layer(s) (Elsheikh et al., 2019). Systematic backpropagation can be used to improve the performance of a neural network, i.e., minimising the mean squared error of outputs. The benefit of the FFBP method is that it enables fast and flexible modelling using only the input variables without requiring additional parameters (Ye and Kim, 2018). The training and evaluation of artificial neural networks (ANNs) were carried out using MATLAB R2020a (MathWorks, 2020) software.

Input and target data were collected involving continuous and semi-continuous plug flow tubular reactor systems based on published papers. The input variables were divided into two main sections: (1) the elemental composition of feedstocks (C (wt.%), H (wt.%), N (wt.%), O (wt.%), S (wt.%)) and (2) process parameters (temperature (°C), pressure (MPa), biomass-to-water ratio (wt.%), residence time (min), catalyst-to-suspension ratio (wt.%)). The target variables were the specific biogas components yields as follow: (*i*) H_2 (mol kg^{-1}), (*ii*) CH_4 (mol kg^{-1}), (*iii*) CO_2 (mol kg^{-1}), (*iv*) CO (mol kg^{-1}), (*v*) C_2H_4 (mol kg^{-1}) and (*vi*) C_2H_6 (mol kg^{-1}). The training data set consisting of 55 groups was compiled using various biomass feedstocks, i.e., corncub, *Spirulina*

Table 4
Life cycle inventory. Functional unit: 1 t of produced biomethanol.

Process/Parameters	Units	Catalytic HTG	Non-catalytic HTG	Data types	Sources
Chemicals production					
N fertiliser (NH_4NO_3)	t	2.849E-01	3.108E-01	Calculation	Dassey et al. (2014)
Energy for N fertiliser production	MWh	4.778E+00	5.194E+00	Ecoinvent v3.4	Ecoinvent (2018)
P fertiliser (ammonium nitrate phosphate)	t	6.070E-02	6.990E-02	Calculation	Dassey et al. (2014)
Energy for P fertiliser production	MWh	3.194E-01	3.694E-01	Ecoinvent v3.4	Ecoinvent (2018)
NaOH catalyst	t	5.517E-01	–	ANN modelling	Current research
Energy for NaOH catalyst production	MWh	1.297E+00	–	Ecoinvent v3.4	Ecoinvent (2018)
Aluminium sulfate flocculant	t	7.259E-02	7.921E-02	Literature-based	Zhu et al. (2020)
Energy for aluminium sulfate production	MWh	2.642E-01	2.889E-01	Ecoinvent v3.4	Ecoinvent (2018)
Biofixation of CO_2					
CO_2 uptake	t	2.188E+00	2.387E+00	Calculation	Pate et al. (2011)
Microalgae feedstock	t	1.452E+00	1.584E+00	Calculation	Current research
Paddlewheels	MWh	3.300E+00	3.600E+00	Calculation	Cheng et al. (2018)
Lamella clarifier and centrifuge	MWh	3.208E-02	3.499E-02	Literature-based	Rogers et al. (2014)
Transportation of feedstock	tkm	1.452E+02	1.584E-01	Calculation	Current research
Hydrothermal Conversion					
Produced Fuel gas	t	1.018E+00	9.951E-01	ANN modelling	Current research
Energy need of HTG	MWh	1.322E+01	1.514E+01	Simulation	Current research
Fuel gas reforming					
The required amount of CO_2	t	6.400E-02	7.400E-02	Simulation	Current research
Required amount of O_2	t	4.643E-02	5.066E-02	Simulation	Current research
Required amount of steam	t	9.368E+01	1.261E+02	Simulation	Current research
Required energy	MWh	4.613E+00	5.685E+00	Simulation	Current research
Water electrolysis					
Mass of required H_2	t	3.630E-02	4.120E-02	Calculation	Current research
The energy need of water electrolysis	MWh	2.053E+00	2.331E+00	Literature-based	Buttler and Spliethoff (2018)
Methanol synthesis					
Required energy	MWh	4.374E+00	4.073E+00	Simulation	Current research
Source of variable renewable energy					
Wind turbines	–	–	–	Ecoinvent v3.4	Ecoinvent (2018)

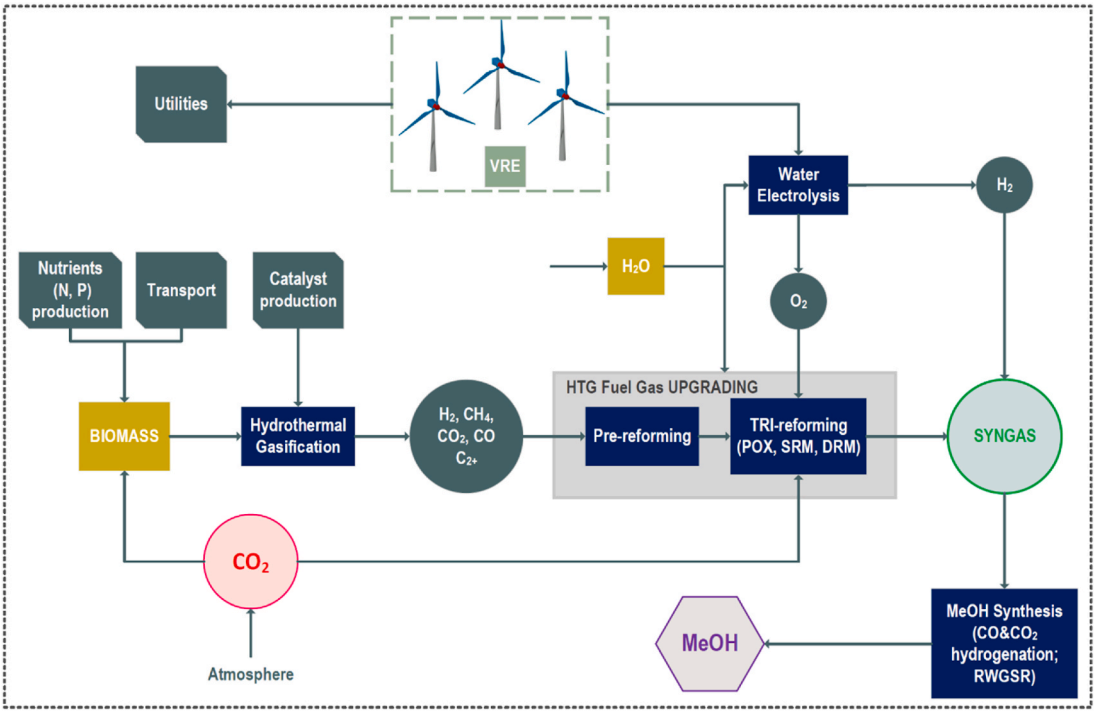

Fig. 2. Life cycle system elements and cradle-to-gate boundary of the biological Power-to-Methanol transformation. N: nitrogen, P: phosphorus, VRE: variable renewable energy, POX: partial oxidation, SRM: steam reforming, DRM: dry reforming, RWGSR: reverse water gas shift reaction.

Table 5
Parameters of biomethanol cost estimation.

Cost element	Functions and parameters	Source
The purchase cost of the heat exchanger (PC_{HX})	$PC_{HX}\ (\$) = \left(\frac{M\&S}{280}\right)\cdot 474.668\cdot A^{0.65}(F_d+F_p)F_m$ (17) F_m = Material correction factor. It is 3.75 for stainless steel. F_d = Design related correction factor. 0.80 for fixed tube sheet. F_p = 0.55 at 6.9 MPa. Extrapolation ($R^2 = 0.959$) was used based on Douglas (1988) to determine its value at 10 MPa (0.93), 26 MPa (2.56) and 27.5 MPa (2.72). Area of HX: $A_{HX}\ (m^2) = \frac{Q}{\Delta T\cdot\beta}$ Q = heat duty (kW); ΔT = temperature difference (−); β = heat transfer coefficient (kW (K m^2)$^{-1}$)	Kharlampidi et al. (2021)
The installed cost of the heat exchanger (IC_{HX})	$IC_{HX}\ (\$) = \left(\frac{M\&S}{280}\right)\cdot 474.668\cdot A^{0.65}((F_d+F_p)F_m+2.29)$ (18)	Kharlampidi et al. (2021)
The purchase cost of the compressor (PC_{COMP})	$PC_{compressor}(\$) = \left(\frac{M\&S}{280}\right)\cdot 664.1(P)^{0.82}F_d$ (19) P = Compression duty (kW) F_d = 1.15 for centrifugal turbine	(Mantingh and Kiss, 2021)
The installed cost of the compressor (IC_{COMP})	$PC_{compressor}(\$) = \left(\frac{M\&S}{280}\right)\cdot 664.1(P)^{0.82}(2.11+F_d)$ (20)	Douglas (1988)
The purchase cost of the reactor (PC_R)	$PC_R(\$) = \left(\frac{M\&S}{280}\right)\cdot 937.636(ID^{1.066}H^{0.802}\cdot F_k$ (21) $F_k = F_zF_x$ F_z = pressure correction factor. The value of F_z is estimated to 16.36 at 26 MPa and 18.11 at 27.5 MPa using polynomial extrapolation ($R^2 = 0.993$) based on Douglas (1988). F_x = material correction factor for pressure vessels, F_x = 3.67 in the case of stainless steel.	Kharlampidi et al. (2021)
The installed cost of the reactor (IC_R)	$IC_R(\$) = \left(\frac{M\&S}{280}\right)\cdot 937.636\cdot ID^{1.066}H^{0.802}\cdot(2.18+F_k)$ (22)	Kharlampidi et al. (2021)
Working hours	8,000 h y^{-1}	Current estimation
Maintenance	1.5% of TPC	Iaquaniello et al. (2018)
General and extraordinary expenses	2% of TPC	Iaquaniello et al. (2018)
CAPEX of H_2 production via water electrolysis	650 € kW_{el}^{-1}	Gorre et al. (2020)
Estimated carbon tax rate	30 € (t CO_2)$^{-1}$	Current estimation
$M\&S_{2018}$ index	1,638.2	Guang et al. (2020)
USD/EUR exchange rate	0.85	Current estimation

platensis microalgae, pinewood, pulp and paper manufacturing derived sludge, *Cladophora glomerata* green algae and *Scenedesmus dimorphus* biomass (as it is listed in the Supplementary Materials).

Levenberg-Marquardt (LM) and Bayesian Regularisation (BR) algorithms were applied for the training of ANNs. The LM method generally requires less training time, while the BR algorithm is suitable to reach good generalisation in the case of small training data sets. Input data were randomly allocated between model training (70%), validation (15%) and testing (15%). The performance and accuracy of ANNs model predictions were assessed based on mean squared error (MSE) (Eq. (23)) and coefficient of determination (R^2) (Eq. (24)).

$$MSE_z = \frac{\sum_{j=1}^{n}\left(Y^z_{pred,j} - Y^z_{exp,j}\right)^2}{n}, \tag{23}$$

$$R^2_z = 1 - \frac{\sum_{j=1}^{n}\left(Y^z_{pred,j} - Y^z_{exp,j}\right)^2}{\sum_{j=1}^{n}\left(Y^z_{exp,j} - \overline{Y}^z_{exp,j}\right)^2}, \tag{24}$$

where $Y^z_{pred,j}$ is the predicted, $Y^z_{exp,j}$ is the experimental, $\overline{Y}^z_{exp,j}$ is the average of all factor level(s) of the zth target variable, and n is the number of data.

The limitations of the developed neural network are in line with the training data set. The HTG process is highly affected by the reactor configuration, operational conditions, type of feedstock and applied catalyst. In this study, ANNs are developed to describe plug-flow tubular reactor systems for the conversion of organic feedstocks. The boundary and applicability of the machine learning model are in the 380–717 °C, 22.5–34.4 MPa, 1–30 wt% biomass-to-water ratio, 0–5.5 wt% CSR with NaOH catalyst load, and 0.3–60.0 min residence time intervals.

3. Results and discussion

3.1. Simulation of hydrothermal gasification with neural networks

Twenty artificial neural network topologies are designed, trained and analysed for the modelling of catalytic and noncatalytic HTG operational units. The examined networks consist of 10 input and 6 target variables. The NN's performance and accuracy are consecutively developed by changing the number of hidden layers and neurons. The examined topologies, performance and accuracy indicators are summarised in Tables 6 and 7.

Satisfactory training results are achieved for 1 hidden layer ANN configurations by applying the Bayesian Regularisation backpropagation method. Raising the number of neurons from 5 to 10 is obtained to be a suitable way to improve both the BR and LM training performances. On the other hand, the testing coefficients of correlations are found to be inadequate in the case of single hidden layer topologies. Adding more neurons (10+) to the ML models has negative effects on validation and testing performances.

Expanding the ANN structure with an additional hidden layer results in significant modelling improvement regarding the mean squared errors and coefficient of correlations. It is obtained that this topology change contributes to reaching high training and testing performances (MSE < 1) by running either the Levenberg-Marquardt or Bayesian Regularisation algorithms. In the case of multiple hidden layers, better testing performances are achieved with the LM backpropagation method. The number of neurons in the hidden layers is adjusted to reduce the mean squared error of the validation process.

The ideal ANN topology for the HTG thermochemical process is illustrated in Fig. 3. It is determined that using 2 hidden layers with 17 neurons in each layer outperforms other topology alternatives. The results show that the LM-10-17-17-6-6 ANN structure is characterised by the best overall training (MSE = 5.680E-01 and R = 0.9822) (Fig. 4a), validation (MSE = 8.249E-01 and R = 0.9974) (Fig. 4b), and testing (MSE = 4.597E-01 and R = 0.9935) (Fig. 4c) performances and accuracies. The developed ideal neural network topology is used to predict the hydrothermal conversion of *Chlorella vulgaris* microalga biomass, improve HTG synthesis gas quality and develop the process synthesis of biomethanol production.

3.2. Process synthesis for biomass-to-methanol transformation

The process flowsheeting diagram of biomethanol production is presented in Fig. 5. The simulation results and stream properties are summarised in Tables S1–S6. Aquatic *Chlorella vulgaris* eukaryotic green algae strain is used for the biofixation of carbon dioxide. Following the cultivation phase, the pre-concentrated wet biomass is converted into a fuel gas mixture using hydrothermal gasification. The aim of the thermochemical conversion stages is the production of high-quality synthesis gas that can be suitably valorised further to a low-carbon intermediate synthetic platform material, i.e., methanol.

The hydrothermal gasification of biomass results in a (1) gas mixture that contains hydrogen, methane, carbon dioxide, carbon monoxide, longer (C_{2+}) alkane and alkene chains and (2) process water with dissolved organic compounds. The constructed artificial neural network enables the detailed investigation of the relationships between the elemental composition of biomass feedstocks, thermochemical process parameters and achievable fuel gas yields. The simulation of catalytic hydrothermal gasification was implemented in the ASPEN Plus process flowsheeting software by applying a yield-type reactor combined with the outputs of the LM-10-17-17-6-6 artificial neural network model. The effects of HTG process parameters on the gas yield and carbon conversion ratio are illustrated in Fig. 6. Damergi et al. (2019) reported that high HTG temperature levels (up to 600 °C) are required in the absence of catalysts to achieve adequate biomass conversion with a carbon conversion efficiency of 41–43%. Our study shows that the carbon conversion ratio and the total gas yield can be increased above 50% and 39 mol kg^{-1} by elevating the temperature from 550 °C to 700 °C (Fig. 6a) at ideal pressure levels (Fig. 6c). The temperature also has a positive effect on methane selectivity, but lower temperature levels are

Table 6
Performance and accuracy comparisons of different ANN structures using Levenberg-Marquardt (LM) training process. The numbers in the ANN topology indicate the number of input variables, neurons in the hidden layer(s), an output layer and target variables.

ANN topology	Training		Validation		Test	
	MSE	R^2	MSE	R^2	MSE	R^2
LM-10-5-6-6	1.531E+00	0.9162	1.563E+00	0.9194	1.595E+00	0.9045
LM-10-10-6-6	4.309E-01	0.9735	1.102E+00	0.9209	5.994E+00	0.8025
LM-10-15-6-6	1.867E+00	0.9018	1.564E+00	0.8988	2.160E+00	0.9004
LM-10-20-6-6	8.531E-01	0.9658	4.119E+00	0.8325	3.626E+00	0.9329
LM-10-8-8-6-6	8.307E-01	0.9551	1.715E+00	0.8978	3.959E+00	0.7825
LM-10-10-10-6-6	4.725E-01	0.9725	2.194E+00	0.8555	1.185E+00	0.9446
LM-10-13-13-6-6	9.054E-01	0.9507	4.812E+00	0.8427	1.795E+00	0.8266
LM-10-17-17-6-6	**5.680E-01**	**0.9647**	**8.249E-01**	**0.9947**	**4.597E-01**	**0.9871**
LM-10-20-20-6-6	2.617E+00	0.8569	4.073E+00	0.8581	5.414E+00	0.7820

Table 7
Performance and accuracy comparisons of different ANN structures using Bayesian Regularisation (BR) training algorithm.

ANN topology	Training		Validation		Test	
	MSE	R^2	MSE	R^2	MSE	R^2
BR-10-5-6-6	4.113E-01	0.9775	–	–	1.504E+00	0.8940
BR-10-8-6-6	6.270E-02	0.9963	–	–	4.013E+00	0.8300
BR-10-10-6-6	2.710E-03	0.9983	–	–	3.858E+00	0.8495
BR-10-15-6-6	6.500E-03	0.9996	–	–	2.540E+00	0.8849
BR-10-20-6-6	2.000E-03	0.9998	–	–	6.695E+00	0.8468
BR-10-5-5-6-6	1.374E-01	0.9924	–	–	1.925E+00	0.9295
BR-10-10-10-6-6	9.600E-02	0.9994	–	–	5.445E+00	0.9018
BR-10-10-13-6-6	8.700E-03	0.9995	–	–	4.419E+00	0.7652
BR-10-17-13-6-6	8.100E-03	0.9995	–	–	3.195E+00	0.8991
BR-10-20-20-6-6	8.600E-03	0.9994	–	–	3.117E+00	0.8765

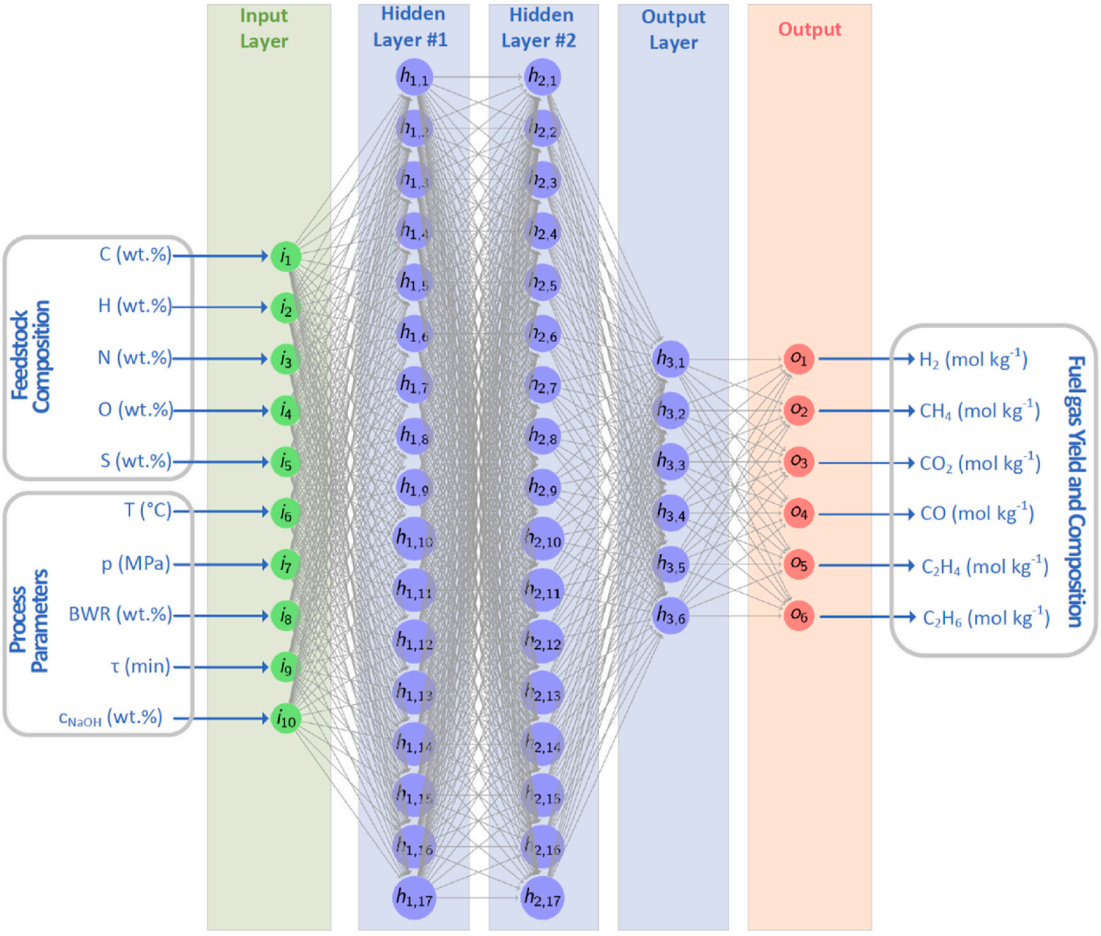

Fig. 3. The ideal LM-10-17-17-6-6 artificial neural network topology for the modelling of hydrothermal gasification. i_i: input variable, o_i: output, $h_{j,k}$: number of kth neuron in the jth layer, T: temperature (°C), p: pressure (MPa), BWR: biomass-to-water ratio (wt.%), τ: residence time (min), c_{NaOH}: NaOH catalyst concentration (wt.%).

favoured to maintain a high hydrogen yield.

The results show that low biomass-to-water levels (≤5 wt%) improve the thermochemical process performance indicators, and BWR has an important role in achieving simultaneously high CCR, gas yields, and hydrogen selectivity (Fig. 6b). The effect of BWR was also confirmed by Leong et al. (2021) who indicated that lower feedstock concentration improves gasification efficiency. Fig. 6c demonstrates that an elevated H_2 evolution rate can be attained by carrying out biomass transformation in a pressure range of 25–27 MPa.

A similar tendency can be described in the case of catalytic hydrothermal conversion, where the H_2 yield can be increased by 29.8% using 1.5 wt% NaOH catalyst load at 625 °C and 27.5 MPa (Fig. 7a). Figs. 6c and 7b and suggest that there is an interaction between pressure and catalyst concentration factors regarding the carbon conversion ratio and H_2 yield. The utilisation of homogeneous catalysis shifts the ideal pressure interval to 28–30 MPa at 625 °C and 12.5 wt% BWR. Fig. 7c shows that residence time has minor effects on the process performance indicators, but lower factor settings are preferred.

Improving and adjusting the hydrothermal conversion is essential for the production of high-quality synthesis gas feedstock. The simulations show that the fuel gas composition, H_2 & CO_2 selectivity and the carbon conversion ratio can be controlled and increased by applying sodium hydroxide homogeneous catalyst, as is illustrated in Fig. 7d. The results suggest that the H_2 yield and CCR can be raised by applying 2 wt% and

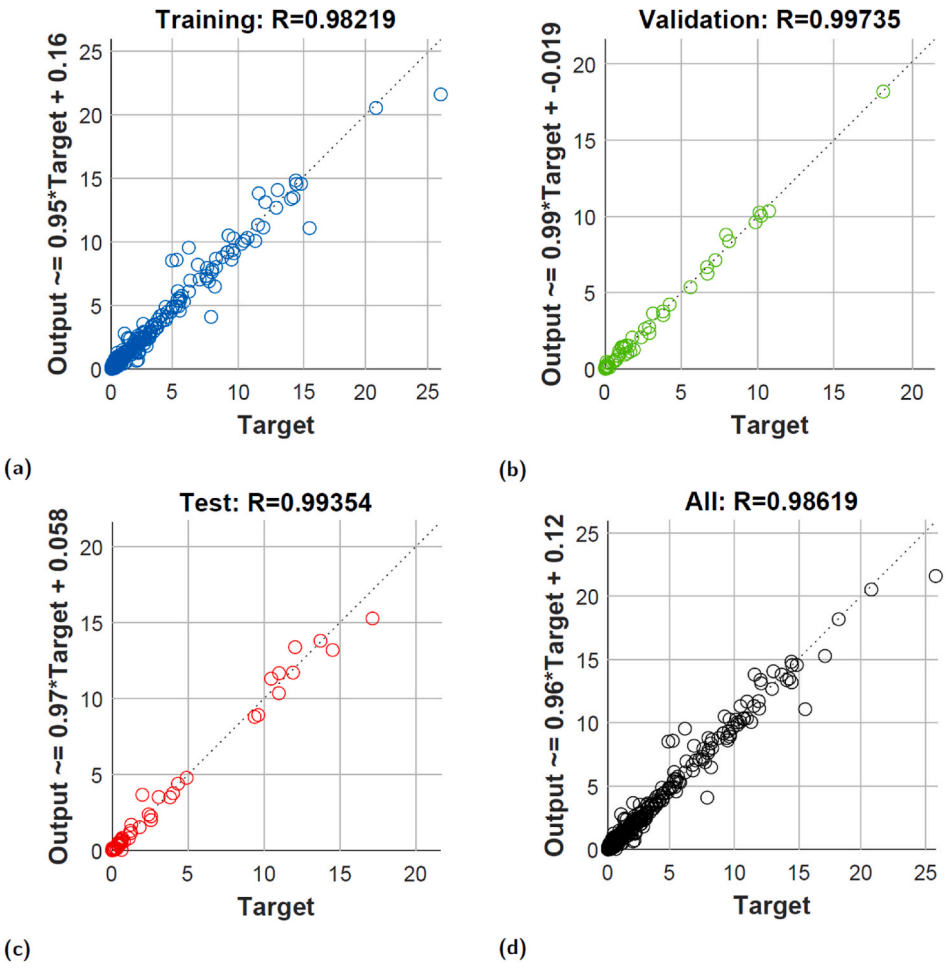

Fig. 4. Accuracy of the LM-10-17-17-6-6 artificial neural network. Coefficients of correlation in the case of neural network's (a) Training, (b) Validation, (c) Test, and (d) All.

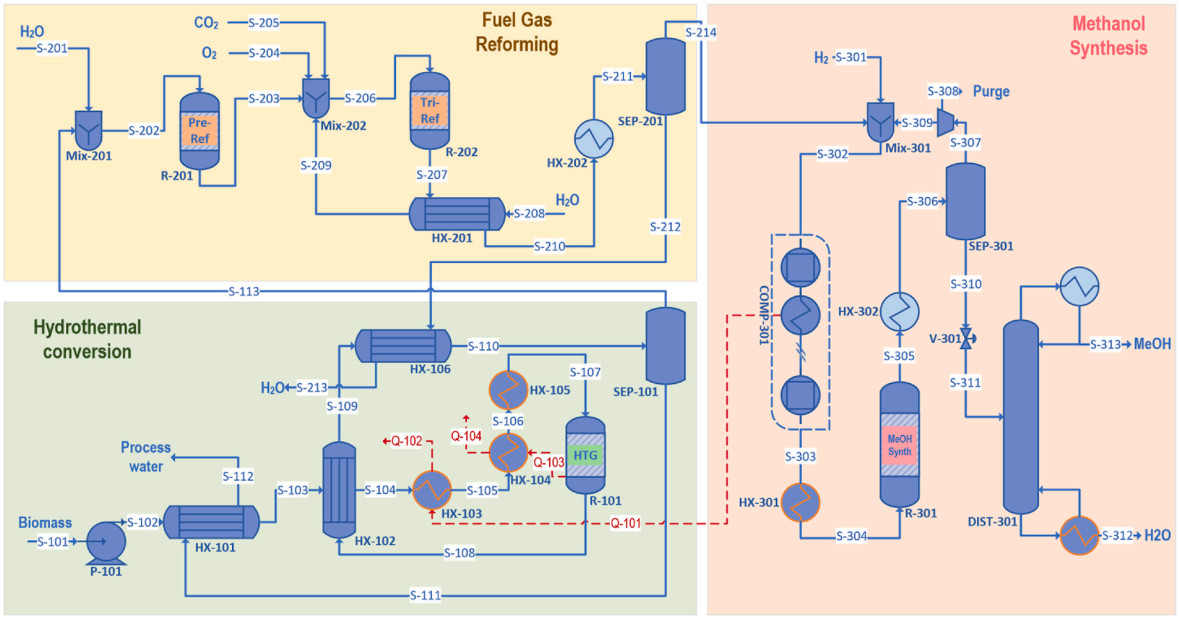

Fig. 5. Process flowsheeting diagram of Power-to-Methanol transformation. P: Pump, HX: heat exchanger, R: Reactor, SEP: separator, Mix: mixer, COMP: compressor, V: valve, D: distillation column, S: stream.

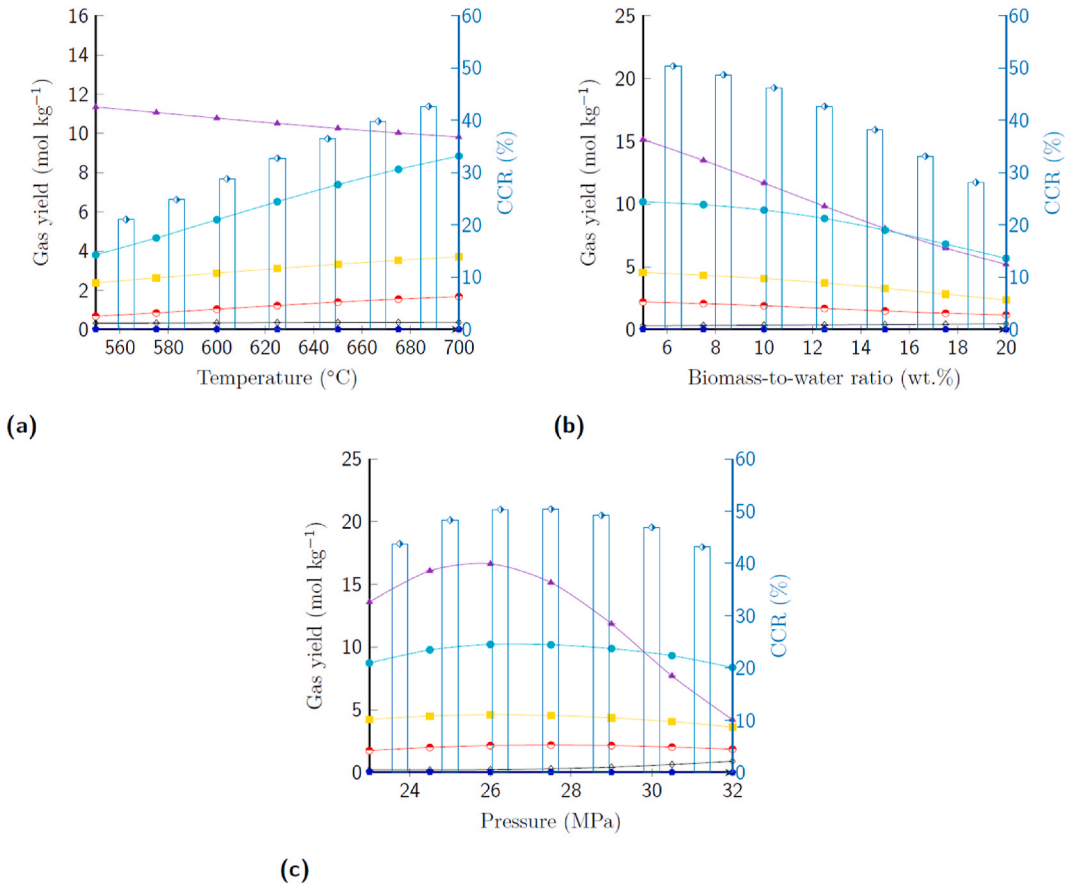

Fig. 6. The effects of HTG process parameters on gas yields and carbon conversion ratio. (a) 27.5 MPa, 12.5 wt% BWR, 2 min residence time; (b) 700 °C, 27.5 MPa, 2 min residence time; (c) 700 °C, 5.0 wt% BWR, 2 min residence time. H_2 (mol kg^{-1}) (—▲—), CH_4 (mol kg^{-1}) (—■—), CO_2 (mol kg^{-1}) (—●—), CO (mol kg^{-1}) (—◇—), C_2H_4 (mol kg^{-1}) (—●—), C_2H_6 (mol kg^{-1}) (—○—), CCR (%) (▯▯). Functional unit: 1 tonne of biomass suspension with 5 wt% dry weight content.

2.5 wt% catalyst loads at 625 °C, respectively. These ANN simulation results are in agreement with the pilot-scale findings of Adar et al. (2020), who reported that the H_2 content of fuel gas could be increased significantly by applying 2 wt% KOH catalyst concentration. The interaction between the biomass-to-water ratio and catalyst load is investigated in the case of total fuel gas yield (Fig. 7e) and carbon conversion ratio (Fig. 7f). Conducting the hydrothermal conversion at an elevated 700 °C temperature level shows that the highest carbon conversion with increased gas yield (39.24 mol kg^{-1}) can be achieved at 5 wt% BWR and 1.9 wt% catalyst concentration.

Using variable renewable energy (e.g., photovoltaic panels and wind turbines) for clean hydrogen generation plays a key role in low-carbon fuels production and decarbonisation of niche applications. In the current system boundary, the renewable H_2 can be supplied from two sources: (*i*) as the main component of HTG fuel gas and (*ii*) external generation involving water electrolysis operational unit. The H_2 yield and synthesis gas selectivity can be influenced during the HTG conversion by (1) applying ideal reaction conditions and (2) homogeneous catalysis. The high flexibility of the hydrothermal valorisation regarding achievable fuel gas composition enables various synthesis gas production scenarios.

In order to achieve adequate synthesis gas feedstock composition defined by the synthesis gas modular (Eq. (10)) and to meet low GHG emission environmental criteria, two main conversions, strategies are distinguished in the flowsheeting process and *ex-ante* sustainability assessment: (1) boosting *in-situ* H_2 evolution in the hydrothermal gasification process by applying sodium hydroxide homogeneous catalyst and (2) enhancing the HTG synthesis gas quality with the integration of H_2 from external water electrolysis supply.

Based on the ANN simulation data, two different hydrothermal reaction conditions are selected for the thermochemical conversion of high moisture containing *Chlorella vulgaris* biomass: (1) catalytic hydrothermal gasification at 700 °C, 27.5 MPa, 5 wt% BWR, 1.9 wt% NaOH catalyst with 2 min residence time in the tubular reactor; and (2) noncatalytic hydrothermal gasification at 700 °C, 26 MPa, 5 wt% BWR, 2 min residence time settings.

Following the biomass transformation, the waste heat content of the high-temperature HTG product stream is recovered in a multi-stage heat exchanger system. The liquid phase and fuel gas products are separated in a phase separator, where the gas mixture is sent to the fuel gas reforming section, and the side product process water is used for additional heat recovery.

The HTG fuel gas mixtures are characterised by low syngas modular (cHTG: $M_{SG} = 0.74$; HTG: $M_{SG} = 0.60$) and contain unwanted side products (hydrocarbons). The fuel gas upgrading process involves two major steps:

(i) Pre-steam reforming is applied to transform the C_{2+} hydrocarbon compounds into synthesis gas.
(ii) In the second step, the excess methane content of the gas stream is converted into syngas by using tri-reforming. It is estimated that the required oxygen for partial oxidation is supplied by water electrolysis as a co-product of H_2 production.

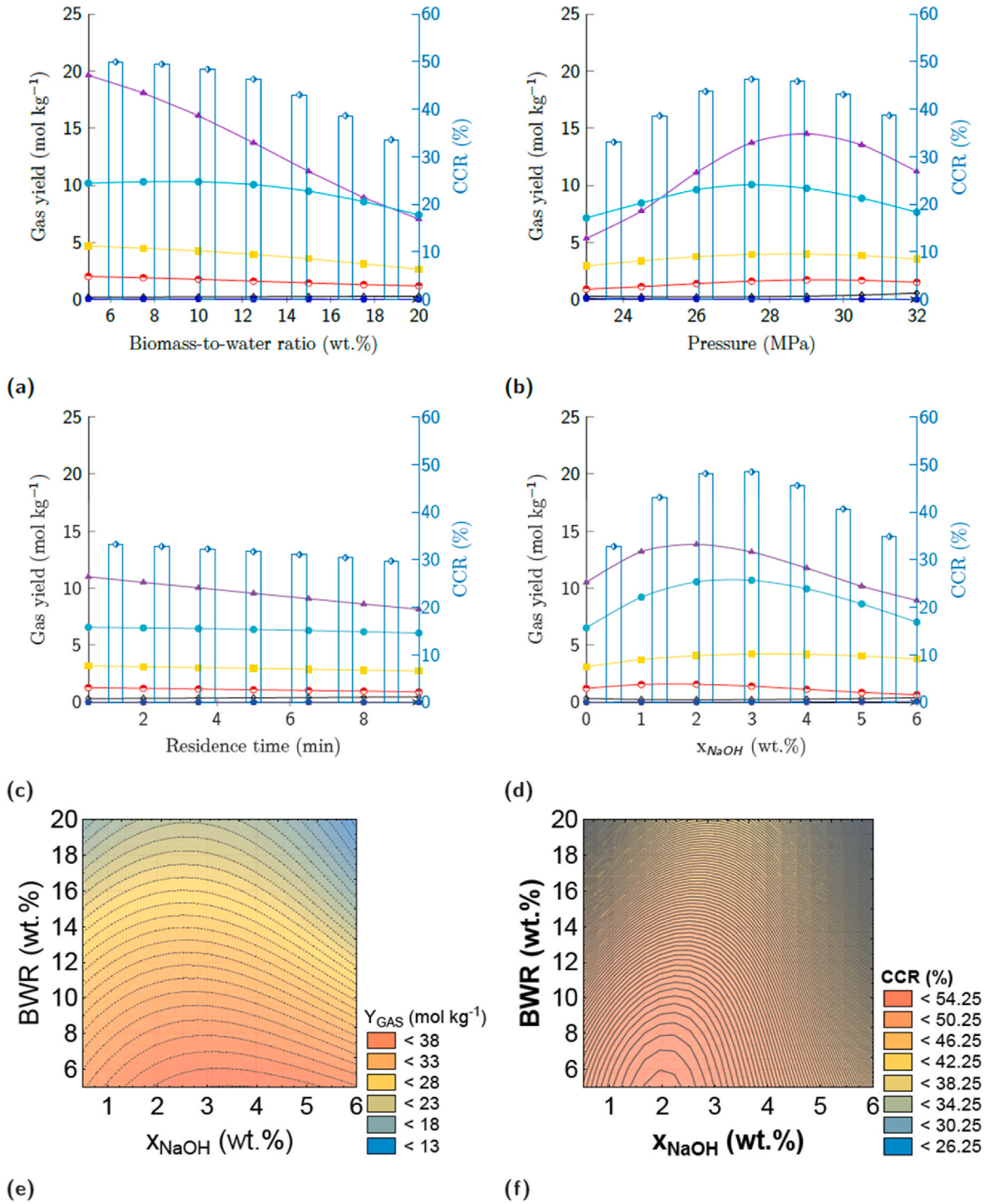

Fig. 7. The effects of cHTG process parameters on gas yields and carbon conversion ratio. (a) 625 °C, 27.5 MPa, 2 min, 1.5 wt% NaOH; (b) 625 °C, 12.5 wt% BWR, 2 min, 1.5 wt% NaOH; (c) 625 °C, 27.5 wt%, 12.5 wt% BWR, 1.5 wt% NaOH; (d) 625 °C, 27.5 MPa, 12.5 wt% BWR, 2 min; (e) 700 °C, 27.5 MPa, 2 min; (f) 700 °C, 27.5 MPa, 2 min. H_2 (mol kg^{-1}) (—▲—), CH_4 (mol kg^{-1}) (—■—), CO_2 (mol kg^{-1}) (—●—), CO (mol kg^{-1}) (—◇—1), C_2H_4 (mol kg^{-1}) (—◆—), C_2H_6 (mol kg^{-1}) (—◓—), CCR (%) (▯▯). Functional unit: 1 tonne of biomass suspension with 5 wt% dry weight content.

The pre-and tri-reforming processes are modelled in Gibbs-reactor units. The effects of reforming parameters are examined on the synthesis gas modular, alkane and alkene conversions to enhance the fuel gas upgrading procedure. Sensitivity analyses are performed to determine ideal reforming conditions, as is summarised in Fig. 8. The simulation results demonstrate that high ethane conversion can be achieved by performing pre-reforming above 400 °C, 20 bar and 1 kmol h^{-1} steam molar flow rate (Fig. 8a and b).

The tri-reforming of cHTG fuel gas serves two main goals:

1. The transformation of methane into synthesis gas, and
2. The adjustment of synthesis gas modular close to ideal levels prior to MeOH synthesis.

The simulations indicate that elevated tri-reforming temperature levels are preferred to enhance methane reforming and the synthesis gas

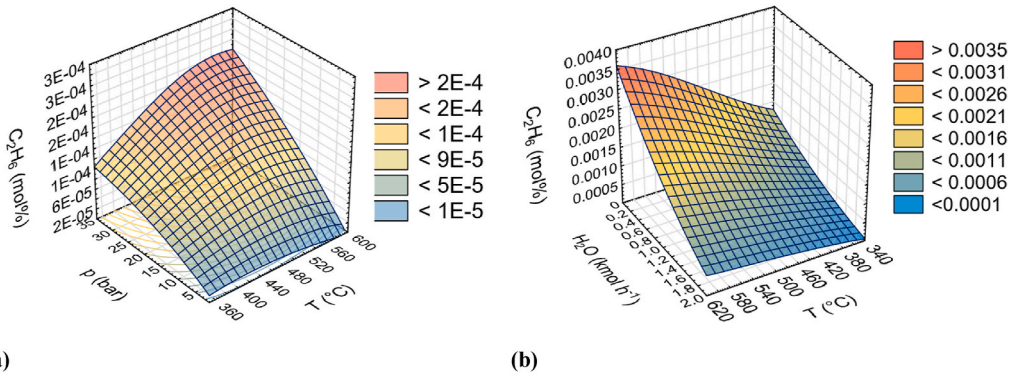

(a) (b)

Fig. 8. Pre-reforming of HTG fuel gas. (a) Effects of temperature and pressure on ethane concentration, (b) Effects of temperature and steam flow rate on ethane concentration.

modular of the S-207 stream. (Fig. 9). Raising steam and oxygen mole flow rates result in high methane conversion (Fig. 9a and c) but augmented oxygen flow rate has negative effects on the value of M_{SG} (Fig. 9b). Fig. 9d presents that the syngas modular can be increased up to 1.75 by adjusting the steam mole flow during the reforming process. It is obtained that the addition of CO_2 does not affect the methane conversion significantly, but it is beneficial to mitigate global warming effects and to fine-tune the level of syngas modular. Fig. 9e illustrates that limiting the CO_2 mole flow rate to an upper constraint of 10 mol h^{-1} contributes to reaching optimal synthesis gas composition prior to methanol production.

The simulation results highlight that a trade-off has to be made between reaching effective methane reforming or the ideal level of synthesis gas modular. It is obtained that maintaining elevated methane conversion results in 1.45 and 1.37 M_{SG} values in the cases of catalytic and noncatalytic HTG fuel gases. For this reason, the resulted product stream of tri-reforming is enriched with H_2 to adjust the synthesis gas composition prior to methanol synthesis. The incorporation of water electrolysis in the biomethanol production chain enables the indirect utilisation of surplus variable renewable electricity produced by wind turbines and photovoltaic panels. In this way, the proposed biomethanol technology can be developed into a Power-to-Liquid decarbonisation process.

The methanol synthesis phase involves multi-stage syngas pressurisation, a continuous reactor with a recirculation system and methanol purification units. The feedstock gas stream is pressurised in 3 stages up to 10 MPa and is fed to a boiling water reactor where three kinetic LHHW reactions are considered:

(i) The hydrogenation of carbon monoxide (Eq. (7))
(ii) The hydrogenation of carbon dioxide (Eq. (8)) and
(iii) Reverse water-gas shift reaction (Eq. (9)).

The unreacted gaseous reagents are stripped and recirculated to the syngas feed. Recycling the unreacted reagents to the reformed syngas product reduces the synthesis gas modular to a value of 1.72. Additional hydrogen is mixed into the syngas feed to achieve the ideal syngas composition for methanol synthesis (where M_{SG} equals approximately 2), as is detailed in Fig. 10a and b.

Sensitivity analyses were performed to maximise methanol yield. It is determined that the highest methanol mole fraction ($x_{CH_3OH} = 0.17$) can be realised at 190 °C (Fig. 10c) using 0.50–0.70 kmol h^{-1} H_2 mole flow rate (Fig. 10d). Finally, the produced methanol and water are separated in a distillation column to obtain a methanol rich stream with high purity ($x_{CH_3OH} > 0.99$).

3.3. Cost estimation of biomethanol production

The total annual cost distribution is illustrated in Fig. 11. The water electrolysis has the highest TAC share reaching 61.1% and 59.2% for the catalytic and noncatalytic HTG cases. The TAC of the hydrothermal conversion process was obtained to be 7.3% higher for the catalytic case. The fuel gas reforming and methanol synthesis stages are also characterised by a higher TAC share compared to the noncatalytic HTG alternative peaking at 1.4% and 2.0%. The total annual costs for the catalytic and noncatalytic process alternatives are obtained to be 316 US$ (t MeOH)$^{-1}$ and 339 US$ (t MeOH)$^{-1}$.

Zhang et al. (2020) investigated the production costs of conventional coal-to-methanol processes and obtained values between 264.0 and 272.6 US $ t^{-1}. The economic aspect of methanol production from natural gas was evaluated by Blumberg et al. (2019) involving various reforming technologies. The levelized cost of methanol was ranged between 198 and 295 US$ t^{-1}. Bellotti et al. (2019) investigated the economic sustainability and feasibility of methanol synthesis using hydrogen and sequestered CO_2. The calculated methanol production cost was assumed to be 324 € t^{-1} (381 US$ t^{-1}) using renewable energy sources in the plant. (Yang et al. (2018)) examined a biomass-to-methanol process alternative using dual-stage entrained flow gasification for the production of bio-syngas. The biomass-to-methanol production cost was in the range of 302–336 US$ t^{-1}.

The results of cost estimation indicate that the production cost of methanol via hydrothermal gasification is in the same range as reported in the case of other biomass-to-methanol scenarios. The economic analysis shows that the utilisation of catalysts in the HTG process is beneficial to reduce the installed equipment cost of hydrothermal conversion by 10.0%. The overall feasibility of biomethanol production could be improved by applying more effective catalysts in the HTG process, and the forthcoming rise in carbon tax (Stevens and Carroll, 2020) could also influence the production costs and margins positively.

3.4. Life cycle impact assessment of power-to-biomethanol alternatives

Multi-perspective sustainability assessments are conducted to quantify the environmental damages of biomass-to-methanol scenarios. According to the intermediate hydrogen generation approach, the life cycle impacts of (1) *in-situ* cHTG H_2 boosting and (2) the utilisation of augmented supply from external sources (i.e., water electrolysis) are investigated as separate process design and LCA scenarios.

The specific greenhouse gas emission of biomethanol alternatives is illustrated by subprocesses in Fig. 12. It is obtained that significant GHG emission reduction can be achieved by both process configurations in a cradle-to-gate system boundary. The utilisation of sodium hydroxide catalyst is beneficial to improve the hydrothermal conversion of

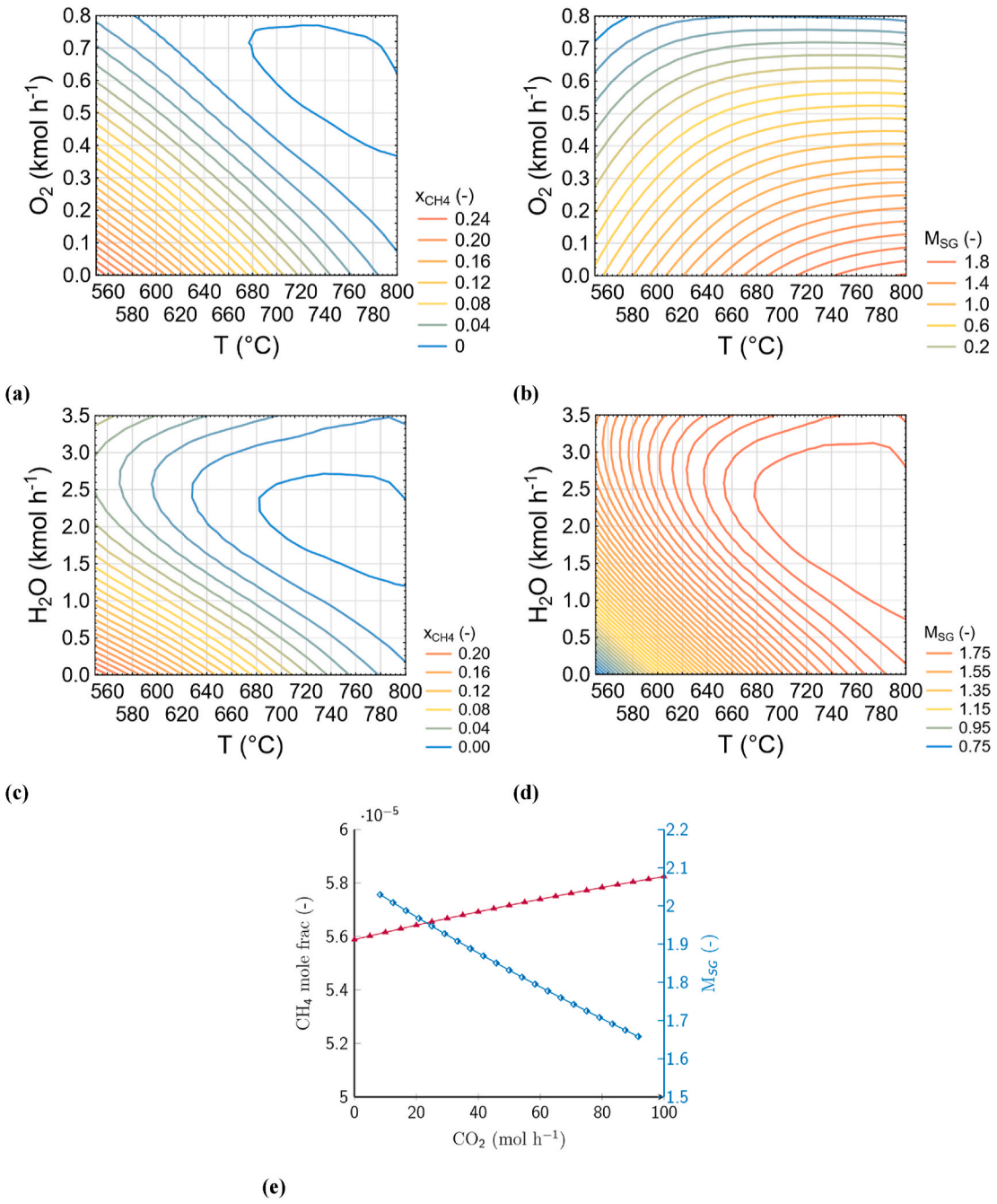

Fig. 9. Tri-reforming of HTG fuel gas. Effects of temperature and O_2 flow rate on (a) methane mole fraction and (b) synthesis gas modular; Interactions between steam mole flow rate and temperature in the case of (c) methane mole fraction and (d) synthesis gas modular at 0.2 MPa; (e) Effects of external CO_2 mole flow on CH_4 mole fraction (—▲—) and synthesis gas modular (—◆—) at 750 °C, 0.2 MPa, 50 mol O_2 h^{-1} and 5 kmol steam h^{-1}. Functional unit: 1 tonne of biomass suspension with 5 wt% dry weight content.

biomass; however, it also elevates the attributed environmental impacts. In the case of the catalytic process, the highest emission rates are coupled with the hydrothermal gasification process (410 kg $CO_{2,eq}$ (t $CH_3OH)^{-1}$) followed by the alkali metal catalyst production (257 kg $CO_{2,eq}$ (t $CH_3OH)^{-1}$). The rest of the processes can be described with a cumulated emission rate of 279 kg $CO_{2,eq}$ (t $CH_3OH)^{-1}$. Using micro-algae strain for the biofixation of CO_2 results in high specific carbon emission uptake (- 1,372 kg $CO_{2,eq}$ (t $CH_3OH)^{-1}$). As it is presented in Fig. 12a, the overall GHG footprint of the catalytic biomass valorisation and methanol production amounts to −439 kg $CO_{2,\ eq}$ (t $CH_3OH)^{-1}$.

Fig. 12b shows that the noncatalytic hydrothermal gasification can be described with a GHG emission rate of 470 kg $CO_{2,eq}$ (t $CH_3OH)^{-1}$ that is followed by the methanol synthesis process (126 kg $CO_{2,eq}$ (t $CH_3OH)^{-1}$), water electrolysis (72 kg $CO_{2,eq}$ (t $CH_3OH)^{-1}$), tri, and pre-reforming of fuel gas (84 and 18 kg $CO_{2,eq}$ (t $CH_3OH)^{-1}$). The cultivation of *Chlorella vulgaris* results in a CO_2 absorption value of 1,500 kg $CO_{2,eq}$ (t $CH_3OH)^{-1}$. The overall greenhouse gas footprint of the LCA alternative is obtained to be −725 kg $CO_{2,eq}$ (t $CH_3OH)^{-1}$. Nguyen et al. (2021) investigated the combination of dry reforming and partial oxidation of methane for the production of methanol and attained a CO_2 emission of 810 kg CO_2 (t $CH_3OH)^{-1}$. Eggemann et al. (2020) examined the global warming potential of 9 Power-to-Fuel systems producing methanol from waste and obtained climate change mitigation potentials between −5.48 and 0.22 kg $CO_{2,eq}$ (kg methanol)$^{-1}$. The LCA results of the present study

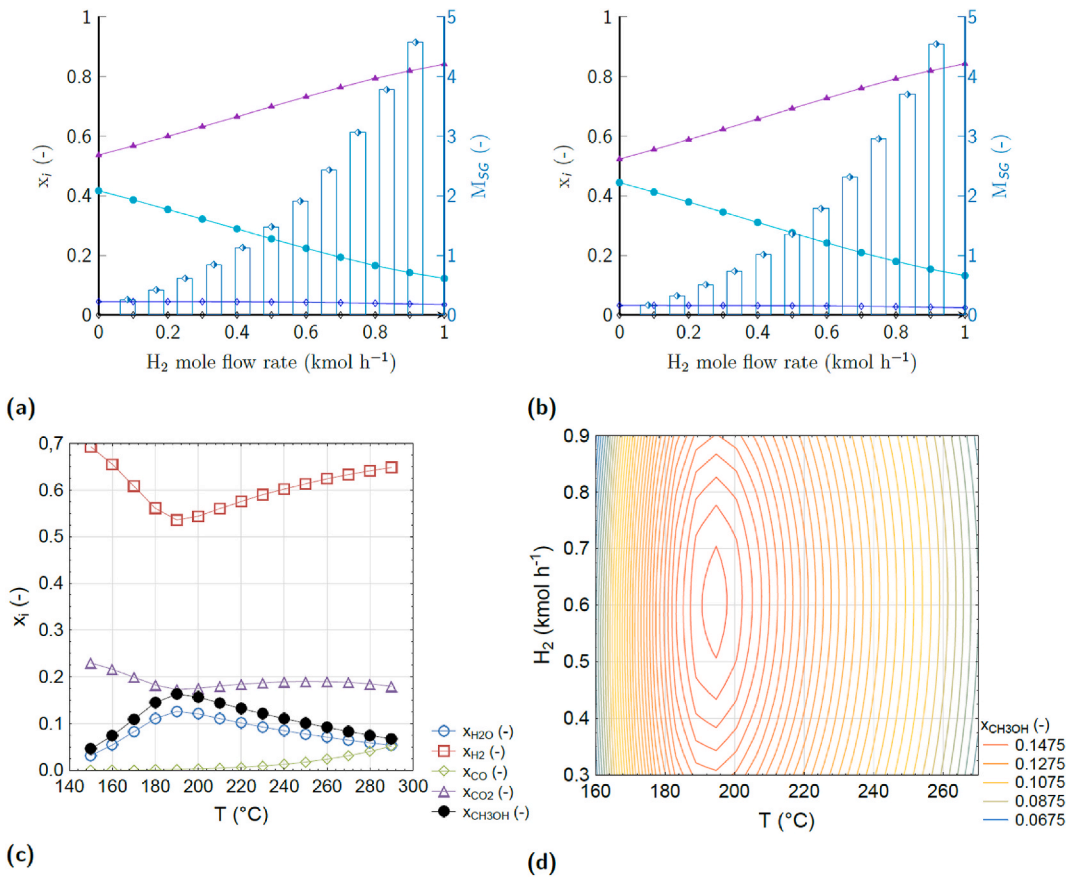

Fig. 10. Reformed HTG fuel gas conversion to methanol. Synthesis gas inlet composition following the recirculation of unreacted regents in the case of (a) catalytic and (b) noncatalytic HTG, (c) biomethanol product stream composition in function of reaction temperature, (d) the effects of external H_2 mole flow rate and temperature on biomethanol mole fraction. x_i: mole fraction (−), $i = H_2$ (−) —▲—; CO (−) —◇—; CO_2 (−) —●—; CH_3OH (−) —◇—. M_{SG} (−) : synthesis gas modular.

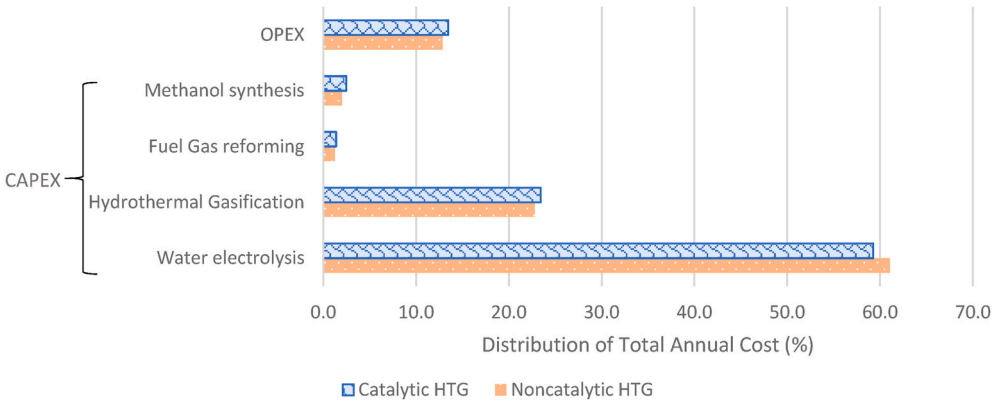

Fig. 11. Total annual cost distribution of biomethanol production using catalytic and noncatalytic hydrothermal gasification.

confirm that low carbon emission synthesis of biomethanol is achievable by converting aquatic biological resources to fuel gas and synthesis gas. Applying catalytic and noncatalytic hydrothermal gasification in the conversion chain open up possibilities by enabling the direct transformation of high moisture containing biomass and waste into value-added products and lowering the greenhouse gas effects of synthetic materials and fuels production.

The life cycle characterisation factors of biomethanol production scenarios are listed by sub-processes in Table 8 and Table 9. The results indicate that fuel gas production and biofixation of CO_2 are environmental bottlenecks in a cradle-to-gate framework. The highest global warming effect (70.1%) is associated with the thermocatalytic conversion of biomass. Supercritical water gasification is also identified as the main contributor to the respiratory inorganics (55.3%) and respiratory organics (42.7%) emission categories (Table 7). The multipurpose environmental screening demonstrates that global warming impacts can be neutralised by involving photosynthetic carbon capture in methanol production. As a side effect, the biofixation of CO_2 elevates terrestrial acidification, where its midpoint share amounts to 52.9%.

The noncatalytic HTG process is rated as one of the major contributors to the overall environmental impacts. Hydrothermal gasification is responsible for 60.1% of the total global warming potential when biomass valorisation is combined with increased external H_2 supply (Table 9). The high GWP of supercritical water gasification was also

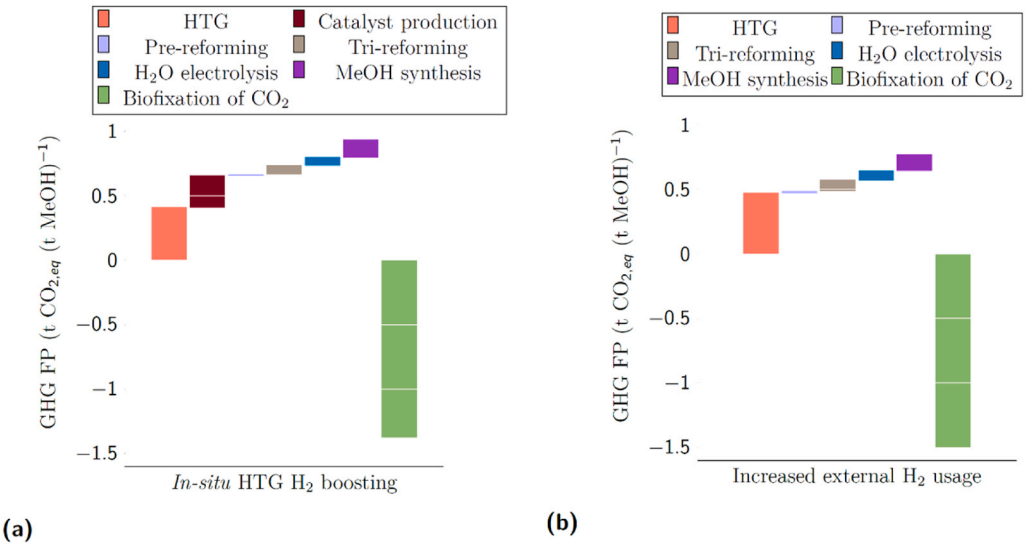

Fig. 12. Cradle-to-gate GHG footprint of biomass-to-methanol alternatives by sub-processes in the cases of (a) *in-situ* HTG H_2 boosting by applying homogeneous catalysis and (b) the combination of augmented external H_2 supply with noncatalytic hydrothermal gasification.

Table 8
Midpoint environmental characterisation factors of biomethanol production in the case of *in-situ* HTG H_2 boosting scenario. The FU is 1 t of produced biomethanol.

Impact category	Unit	*In-situ* HTG H_2 boosting via catalytic conversion						
		Water Electrolysis	cHTG	MeOH Synthesis	Pre-reforming	Tri-reforming	CO_2 Biofixation	Total
Carcinogens	kg $C_2H_3Cl_{eq}$	2.78E+00	1.80E+01	5.92E+00	3.96E-01	5.84E+00	1.43E+01	4.72E+01
Non-carcinogens	kg $C_2H_3Cl_{eq}$	6.30E+00	4.09E+01	1.34E+01	8.98E-01	1.32E+01	2.50E+01	9.98E+01
Respiratory inorganics	kg $PM_{2.5,eq}$	1.25E-01	1.05E+01	2.66E-01	1.78E-02	2.63E-01	1.01E+00	2.74E+00
Ionizing radiation	Bq C-14_{eq}	5.25E+02	9.05E+03	1.12E+03	7.48E+01	1.10E+03	4.50E+03	1.64E+04
Ozone layer depletion	kg CFC-11_{eq}	8.62E-06	1.07E-04	1.84E-05	1.23E-06	1.81E-05	7.74E-05	2.31E-04
Respiratory organics	kg $C_2H_{4,eq}$	3.88E-02	2.80E-01	8.27E-02	5.53E-03	8.16E-02	1.68E-01	6.56E-01
Aquatic ecotoxicity	kg TEG water	1.66E+04	1.07E+05	3.54E+04	2.37E+03	3.50E+04	1.06E+05	3.02E+05
Terrestrial ecotoxicity	kg TEG soil	5.48E+03	3.55E+04	1.17E+04	7.81E+02	1.15E+04	1.82E+04	8.32E+04
Terrestrial acid/nutri	kg $SO_{2,eq}$	1.60E+00	1.43E+01	3.40E+00	2.28E-01	3.36E+00	2.57E+01	4.86E+01
Land occupation	m^2org.arable	2.41E+00	1.56E+01	5.14E+00	3.44E-01	5.08E+00	9.69E+00	3.82E+01
Aquatic acidification	kg $SO_{2,eq}$	5.69E-01	5.40E+00	1.21E+00	8.12E-02	1.20E+00	5.54E+00	1.40E+01
Aquatic eutrophication	kg PO_4 P-lim	1.17E-01	7.55E-01	2.48E-01	1.66E-02	2.45E-01	3.84E-01	1.77E+00
Global warming	kg $CO_{2,eq}$	6.37E+01	6.54E+02	1.36E+02	9.09E+00	7.01E+01	−1.37E+03	−4.39E+02
Non-renewable energy	MJ primary	8.10E+02	9.59E+03	1.72E+03	1.15E+02	1.70E+03	9.24E+03	2.32E+04
Mineral extraction	MJ surplus	5.25E+01	3.38E+02	1.12E+02	7.49E+00	1.11E+02	1.99E+02	8.20E+02

Table 9
Midpoint environmental characterisation factors of biomethanol production in the case of increased external H_2 usage LCA alternative. The FU is 1 t of produced biomethanol.

Impact category	Unit	Increased external H_2 usage						
		Water Electrolysis	HTG	MeOH Synthesis	Pre-reforming	Tri-reforming	CO_2 Biofixation	Total
Carcinogens	kg $C_2H_3Cl_{eq}$	3.15E+00	2.05E+01	5.51E+00	7.98E-01	6.89E+00	1.56E+01	5.24E+01
Non-carcinogens	kg $C_2H_3Cl_{eq}$	7.15E+00	4.64E+01	1.25E+01	1.81E+01	1.56E+01	2.72E+01	1.11E+02
Respiratory inorganics	kg $PM_{2.5,eq}$	1.42E-01	9.21E-01	2.48E-01	3.59E-02	3.10E-01	1.11E+00	2.76E+00
Ionizing radiation	Bq C-14_{eq}	5.96E+02	3.87E+03	1.04E+03	1.51E+02	1.30E+03	4.91E+03	1.19E+04
Ozone layer depletion	kg CFC-11_{eq}	9.78E-06	6.36E-05	1.71E-05	2.48E-06	2.14E-05	8.45E-05	1.99E-04
Respiratory organics	kg C_2H_{4eq}	4.41E-02	2.86E-01	7.70E-02	1.11E-02	9.63E-02	1.83E-01	6.97E-01
Aquatic ecotoxicity	kg TEG water	1.89E+04	1.23E+05	3.30E+04	4.77E+03	4.12E+04	1.15E+05	3.36E+05
Terrestrial ecotoxicity	kg TEG soil	6.22E+03	4.04E+04	1.09E+04	1.57E+03	1.36E+04	1.99E+04	9.26E+04
Terrestrial acid/nutri	kg $SO_{2,eq}$	1.81E+00	1.18E+01	3.17E+00	4.59E-01	3.97E+00	2.80E+01	4.92E+01
Land occupation	m^2org.arable	2.74E+00	1.78E+01	4.79E+00	6.94E-01	5.99E+00	1.06E+01	4.26E+01
Aquatic acidification	kg $SO_{2,eq}$	6.46E-01	4.20E+00	1.13E+00	1.64E-01	1.41E+00	6.05E+00	1.36E+01
Aquatic eutrophication	kg PO_4 P-lim	1.32E-01	8.60E-01	2.31E-01	3.35E-02	2.89E-01	4.19E-02	1.97E+00
Global warming	kg $CO_{2,eq}$	7.24E+01	4.70E+02	1.26E+02	1.83E+01	8.42E+01	−1.50E+03	−7.25E+02
Non-renewable energy	MJ primary	9.19E+02	5.97E+03	1.61E+03	2.33E+02	2.01E+03	1.01E+04	2.08E+04
Mineral extraction	MJ surplus	5.96E+01	3.87E+02	1.04E+02	1.51E+01	1.30E+02	2.17E+02	9.14E+02

suggested in former studies in the cases of corn stalks (Wang et al., 2019) and coal (Chen et al., 2019a). In addition, it is obtained that the fuel gas production stage has the highest share regarding aquatic eutrophication (43.8%), terrestrial ecotoxicity (43.7%) and mineral extraction (42.7%) damage categories. The biomass cultivation stage has a negative overall global warming potential because of the high CO_2 utilisation rate during

the metabolism of photosynthetic eukaryotic microalgae cells. On the other hand, the production and utilisation of fertilisers induce significant environmental impacts on terrestrial acidification (56.9%), application of non-renewable energies (48.4%), aquatic acidification (44.5%) and ozone layer depletion (42.5%) characterisation factors.

The mid- and endpoint environmental impacts of biomethanol production alternatives are illustrated in Fig. 13. The highest life cycle impacts are coupled with the emission of respiratory inorganics and non-carcinogen compounds, the utilisation of non-renewable energy, global warming potential and terrestrial ecotoxicity (Fig. 13a). The performed sustainability assessments demonstrate that the *in-situ* H_2 boosting strategy tends to be a more favourable LCA scenario maintaining negative climate change effects and achieving lower damages on human health and ecosystem quality by 2.7% and 10.6% (Fig. 13b). Increasing the external H_2 utilisation results in significantly better decarbonisation potentials, where the climate change effect and resources utilisation can be decreased by 65.5% and 10.4%.

The modelling of the HTG process with an artificial neural network showed that the catalytic upgrading of biomass is a suitable method to enhance H_2 selectivity, carbon recovery and fuel gas yield. The improved thermochemical conversion decreases the required amount of biomass feedstock by 9.1% to 1.452 t algae (t MeOH)$^{-1}$ and, as an after effect, the utilisation of fertilisers. This conversion-related benefit results in lower environmental burdens on human health and ecosystem quality endpoint subfactors (Fig. 13b). The application of sodium hydroxide homogeneous catalyst elevates climate change impacts, and the endpoint damages of biomethanol production by 78.6 IMPACT 2002+ mPt (t MeOH)$^{-1}$ that is 14.5% of the total impacts. The high specific global warming potential of alkali catalyst utilisation calls the attention for developing and screening applicable catalysts for hydrothermal conversions considering both reaction performance indicators and environmental criteria.

The performed *ex-ante* sustainability assessments highlight that combining the biofixation of CO_2 and flexible fuel gas production are advantageous technological pairing in decarbonisation applications. The biomass-to-methanol valorisation via hydrothermal gasification is characterised by a negative greenhouse gas footprint indicating strong CO_2 removal and low-emissions carbon fuel production potentials. The integration of controlled biogas generation into the Power-to-Fuel process schemes enables effective biomass valorisation, the production of low-carbon synthetic fuels and materials and the indirect reduction of GHG emissions.

4. Conclusions

The biomethanol is a valuable intermediate product, a platform molecule that can be used for the production of low-carbon emission fuels and materials. The sustainability of biomethanol production is evaluated by applying machine learning, process flowsheeting and life cycle assessment computational tools. Process synthesis is carried out by transforming high moisture containing microalgae biomass into synthesis gas and biomethanol in sequential thermochemical steps.

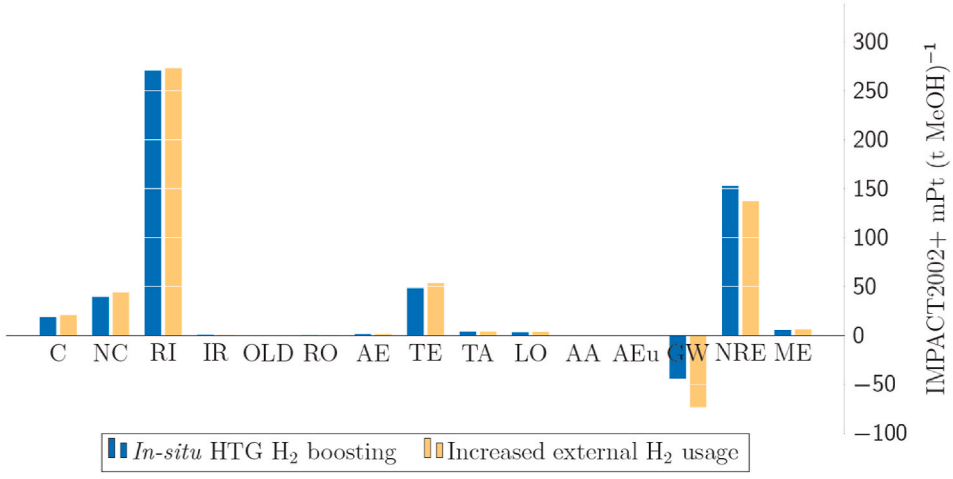

(a)

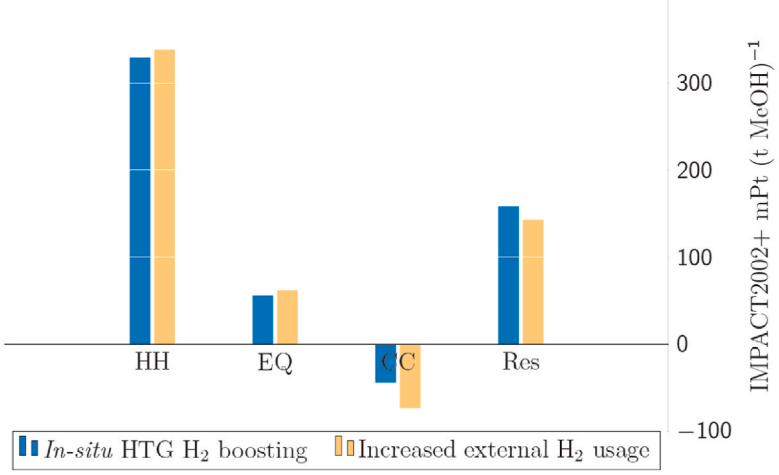

(b)

Fig. 13. Multi-purpose life cycle assessment of bio-methanol production in a cradle-to-gate framework. (a) Midpoint and (b) Endpoint environmental impacts. C: Carcinogens; NC: Non-carcinogens; RI: Respiratory inorganics; IR: Ionizing radiation; OLD: Ozone layer depletion; RO: Respiratory organics; AE: Aquatic ecotoxicity; TE: Terrestrial ecotoxicity; TA: Terrestrial acid/nutri; LO: Land occupation; AC: Aquatic acidification; AEu: Aquatic eutrophication; GW: Global warming; NRE: Non-renewable energy; ME: Mineral extraction. HH: Human Health; EQ: Ecosystem quality; CC: Climate change; Res: Resources.

Artificial neural network (ANN) models are developed for the simulation of catalytic and noncatalytic hydrothermal gasification unit operations. *Ex-ante* cradle-to-gate life cycle assessments indicate that strong decarbonisation potentials can be achieved by involving the biofixation of CO_2 and hydrothermal valorisation in the Power-to-Liquid conversion chain. Hydrogen generation strategies have an important role in achieving close carbon-neutral emission rates. The in-process flexibility of hydrothermal gasification and the use of renewable hydrogen contribute to decreasing the GHG footprint of biomethanol production by 65.1% and the overall endpoint impacts by 6.2%. The process economic analysis shows that the production cost of biomethanol via hydrothermal gasification and fuel gas upgrading ranges between 316 and 339 US$ (t MeOH)$^{-1}$ depending on the applied hydrogen supply strategy. The biomethanol production based on supercritical water gasification offers an attractive option for (*i*) carbon dioxide utilisation, (*ii*) valorisation of biomass and (*iii*) decarbonisation of conventional processes.

CRediT authorship contribution statement

Dániel Fózer: Investigation, Conceptualization, Formal analysis, Visualization, Writing – original draft. **András József Tóth:** Funding acquisition, Data curation. **Petar Sabev Varbanov:** Methodology, Writing – review & editing. **Jiří Jaromír Klemeš:** Funding acquisition, Methodology, Writing – review & editing. **Péter Mizsey:** Funding acquisition, Methodology, Writing – review & editing.

Declaration of competing interest

The authors declare that they have no known competing financial interests or personal relationships that could have appeared to influence the work reported in this paper.

Acknowledgement

This work was supported by the ÚNKP-20-4-II-BME-296 new national excellence program of the ministry for innovation and technology from the source of the national research, development and innovation fund and the NTP-NFTÖ-20-B-0095 National Talent Program. The authors are grateful for the financial support from the Hungarian National Scientific Research Foundation (OTKA) projects: nr.: 128543 and nr.: 131586. The research reported in this paper and carried out at BME has been supported by the NRDI Fund (TKP2020 NC, Grant No. BME-NC) based on the charter of bolster issued by the NRDI Office under the auspices of the Ministry for Innovation and Technology. The research was supported by the EU LIFE program, LIFE-CLIMCOOP project (LIFE19 CCA/HU/001320). The EU project Sustainable Process Integration Laboratory – SPIL, funded as project No. CZ.02.1.01/0.0/0.0/15 003/0000456, by Czech Republic Operational Programme Research and Development, Education is also gratefully acknowledged under the collaboration agreement with the University of Miskolc.

Appendix A. Supplementary data

Supplementary data to this article can be found online at https://doi.org/10.1016/j.jclepro.2021.128606.

Nomenclature

a_i	Pre-exponential factor
ANN	Artificial Neural Network
BR	Bayesian Regularisation
BTM	Biomass-to-methanol
BWR	Biomass-to-Water Ratio (wt.%)
CCR	Carbon Conversion Ratio (−)
cHTG	Catalytic Hydrothermal Gasification
CRF	Capital Recovery Factor
DRM	Dry Reforming
E_a	Apparent activation energy (J mol^{-1})
FC	Fixed Carbon (wt.%)
FFBP	Feed-Forward Back Propagation
f_k	Fugacity of the component (Pa)
FP	Footprint
FU	Functional Unit
GHG	Greenhouse Gas
GWP	Global Warming Potential
HTG	Hydrothermal Gasification
IC_i	The installed cost of the ith equipment
k_i	Kinetic factor
$K_{A,B,C}$	Equilibrium constants of reactions
K_k	Adsorption equilibrium constant of component k (Pa^{-1})
LCA	Life Cycle Assessment
LCIA	Life Cycle Impact Assessment
LHHW	Langmuir-Hinshelwood-Hougen-Watson
LM	Levenberg-Marquardt
M&S	Marshall and Swift index
ML	Machine Learning
MLP	Multilayer Perceptron
MSE	Mean Squared Error
M_{SG}	Synthesis gas modular (−)
P2L	Power-to-Liquid
PC_i	The purchase cost of the ith equipment
POX	Partial Oxidation
r_i	Reaction rate
RWGS	Reverse Water Gas Shift Reaction
SRM	Steam Reforming
TAC	Total Annual Cost (€ y^{-1})
TPC	Total Plant Cost (€)
VM	Volatile Matter (wt.%)
VRE	Variable Renewable Energy
x_{CH4}	Mole fraction of methane (−)
Y_{GAS}	Total gas yield (mol kg^{-1})
Z_i	Mole fraction of H_2, CO_2, CO (−)

References

Abdpour, S., Santos, R.M., 2021. Recent advances in heterogeneous catalysis for supercritical water oxidation/gasification processes: insight into catalyst development. Process Saf. Environ. Protect. 149, 169–184. https://doi.org/10.1016/j.psep.2020.10.047.

Adar, E., Ince, M., Bilgili, M.S., 2020. Supercritical water gasification of sewage sludge by continuous flow tubular reactor: a pilot scale study. Chem. Eng. J. 391, 123499 https://doi.org/10.1016/j.cej.2019.123499.

Adnan, M.A., Kibria, M.G., 2020. Comparative techno-economic and life-cycle assessment of power-to-methanol synthesis pathways. Appl. Energy 278, 115614. https://doi.org/10.1016/j.apenergy.2020.115614.

APEA, 2021. Aspen Process Economic Analyzer. In: aspentech.com/en/products/pages/aspen-process-economic-analyzer. (Accessed 12 July 2021).

AspenTech, 2020. ASPEN Plus®. aspentech.com/en/products/engineering/aspen-plus. (Accessed 9 January 2021). Accessed.

Bai, B., Wang, W., Jin, H., 2020. Experimental study on gasification performance of polypropylene (PP) plastics in supercritical water. Energy 191, 116527. https://doi.org/10.1016/j.energy.2019.116527.

Bellotti, D., Cassettari, L., Mosca, M., Magistri, L., 2019. RSM approach for stochastic sensitivity analysis of the economic sustainability of a methanol production plant using renewable energy sources. J. Clean. Prod. 240, 117947 https://doi.org/10.1016/j.jclepro.2019.117947.

Belotti, G., de Caprariis, B., De Filippis, P., Scarsella, M., Verdone, N., 2014. Effect of *Chlorella vulgaris* growing conditions on bio-oil production via fast pyrolysis. Biomass Bioenergy 61, 187–195. https://doi.org/10.1016/j.biombioe.2013.12.011.

Bhatia, S.K., Bhatia, R.K., Jeon, J.M., Kumar, G., Yang, Y.H., 2019. Carbon dioxide capture and bioenergy production using biological system – a review. Renew. Sustain. Energy Rev. 110, 143–158. https://doi.org/10.1016/j.rser.2019.04.070.

Blumberg, T., Lee, Y.D., Morosuk, T., Tsatsaronis, G., 2019. Exergoenvironmental analysis of methanol production by steam reforming and autothermal reforming of natural gas. Energy 181, 1273–1284. https://doi.org/10.1016/j.energy.2019.05.171.

Butera, G., Jensen, S.H., Ahrenfeldt, J., Clausen, L.R., 2021. Techno-economic analysis of methanol production units coupling solid oxide cells and thermochemical biomass

conversion via the TwoStage gasifier. Fuel Process. Technol. 215, 106718 https://doi.org/10.1016/j.fuproc.2020.106718.
Buttler, A., Spliethoff, H., 2018. Current status of water electrolysis for energy storage, grid balancing and sector coupling via power-to-gas and power-to-liquids: a review. Renew. Sustain. Energy Rev. 82, 2440–2454. https://doi.org/10.1016/j.rser.2017.09.003.
Cerinski, D., Baleta, J., Mikulčić, H., Mikulandrić, R., Wang, J., 2020. Dynamic modelling of the biomass gasification process in a fixed bed reactor by using the artificial neural network. Clean. Eng. Technol., 100029 https://doi.org/10.1016/j.clet.2020.100029.
Chen, J., Xu, W., Zhang, F., Zuo, H., Jiaqiang, E., Wei, K., Liai, G., Fan, Y., 2019a. Thermodynamic and environmental analysis of integrated supercritical water gasification of coal for power and hydrogen production. Energy Convers. Manag. 198, 111927 https://doi.org/10.1016/j.enconman.2019.111927.
Chen, J., Xu, W., Zuo, H., Wu, X., E, J., Wang, T., Zhang, F., Lu, N., 2019b. System development and environmental performance analysis of a solar-driven supercritical water gasification pilot plant for hydrogen production using life cycle assessment approach. Energy Convers. ManagClean. Eng. Technol. 184, 60–73. https://doi.org/10.1016/j.enconman.2019.01.041.
Chen, Q., Gu, Y., Tang, Z., Sun, Y., 2019c. Comparative environmental and economic performance of solar energy integrated methanol production systems in China. Energy Convers. Manag. 187, 63–75. https://doi.org/10.1016/j.enconman.2019.03.013.
Cheng, J., Guo, W., Ameer Ali, K., Ye, Q., Jin, G., Qiao, Z., 2018. Promoting helix pitch and trichome length to improve biomass harvesting efficiency and carbon dioxide fixation rate by *Spirulina sp.* in 660 m^2 raceway ponds under purified carbon dioxide from a coal chemical flue gas. Bioresour. Technol. 261, 76–85. https://doi.org/10.1016/j.biortech.2018.04.017.
Csányi, G., Willatt, M.J., Ceriotti, M., 2020. Machine-Learning of Atomic-Scale Properties Based on Physical Principles. Springer International Publishing, Cham, Switzerland, pp. 99–127. https://doi.org/10.1007/978-3-030-40245-7_6.
Čuček, L., Klemeš, J.J., Kravanja, Z., 2011. Overview of footprints and relations between carbon and nitrogen footprints. Chem. Eng. Trans. 25, 923–928. https://doi.org/10.3303/CET1125154.
Čuček, L., Varbanov, P.S., Klemeš, J.J., Kravanja, Z., 2012. Total footprints-based multicriteria optimisation of regional biomass energy supply chains. Energy 44, 135–145. https://doi.org/10.1016/j.energy.2012.01.040.
Damergi, E., Madi, H., Sharma, S., Boukis, N., Marechal, F., Van Herle, J., Ludwig, C., 2019. A combined hydrothermal gasification - solid oxide fuel cell system for sustainable production of algal biomass and energy, 41, 101552. https://doi.org/10.1016/j.algal.2019.101552.
Dassey, A.J., Hall, S.G., Theegala, C.S., 2014. An analysis of energy consumption for algal biodiesel production: comparing the literature with current estimates. Algal Res. 4, 89–95. https://doi.org/10.1016/j.algal.2013.12.006.
Deng, X., Lv, T., 2020. Power system planning with increasing variable renewable energy: a review of optimisation models. J. Clean. Prod. 246, 118962 https://doi.org/10.1016/j.jclepro.2019.118962.
dos Santos, P.F., Pereira, C.G., 2021. Study of the gasification process of liquid biomasses in supercritical water using a thermodynamic mathematical model. J. Supercrit. Fluids 168, 105049. https://doi.org/10.1016/j.supflu.2020.105049.
Douglas, J.M., 1988. Conceptual Design of Chemical Processes. McGraw-Hill Publishing Co., New York, United States of America, ISBN 978-0071001953.
Dvoretsky, D., Dvoretsky, S., Temnov, M., Akulinin, E., Markin, I., Ustinskaya, Y., Yeskova, M., Meronyuk, K., 2020. Research into the influence of cultivation conditions on the fatty acid composition of lipids of Chlorella vulgaris microalgae. Chem. Eng. Trans. 79, 31–36. https://doi.org/10.3303/CET2079006.
Ecoinvent, 2018. Ecoinvent Database v3.4: Life Cycle Inventory Database v34.ecoquery.ecoinvent.org/Details/PDF/214562A8-2093-4303-A1DC29DF46FFE06E/06590A66-662A-4885-8494-AD0CF410F956. (Accessed 9 January 2021). accessed.
Eggemann, L., Escobar, N., Peters, R., Burauel, P., Stolten, D., 2020. Life cycle assessment of a small-scale methanol production system: a Power-to-Fuel strategy for biogas plants. J. Clean. Prod. 271, 122476 https://doi.org/10.1016/j.jclepro.2020.122476.
Elsheikh, A.H., Sharshir, S.W., Abd Elaziz, M., Kabeel, A., Guilan, W., Haiou, Z., 2019. Modeling of solar energy systems using artificial neural network: a comprehensive review. Sol. Energy 180, 622–639. https://doi.org/10.1016/j.solener.2019.01.037.
Fan, Y.V., Lee, C.T., Lim, J.S., Klemeš, J.J., Le, P.T.K., 2019. Cross-disciplinary approaches towards smart, resilient and sustainable circular economy. J. Clean. Prod. 232, 1482–1491. https://doi.org/10.1016/j.jclepro.2019.05.266.
Fózer, D., Volanti, M., Passarini, F., Varbanov, P.S., Klemeš, J., Mizsey, P., 2020. Bioenergy with carbon emissions capture and utilisation towards GHG neutrality: power-to-Gas storage via hydrothermal gasification. Appl. Energy 280, 115923. https://doi.org/10.1016/j.apenergy.2020.115923.
Gautam, P., Upadhyay, S. Neha, Dubey, S., 2020. Bio-methanol as a renewable fuel from waste biomass: current trends and future perspective. Fuel 273, 117783. https://doi.org/10.1016/j.fuel.2020.117783.
Gonçalves Neto, J., Vidal Ozorio, L., Campos de Abreu, T.C., Ferreira dos Santos, B., Pradelle, F., 2021. Modeling of biogas production from food, fruits and vegetables wastes using artificial neural network (ANN). Fuel 285, 119081. https://doi.org/10.1016/j.fuel.2020.119081.
Gorre, J., Ruoss, F., Karjunen, H., Schaffert, J., Tynjälä, T., 2020. Cost benefits of optimizing hydrogen storage and methanation capacities for Power-to-Gas plants in dynamic operation. Appl. Energy 257, 113967. https://doi.org/10.1016/j.apenergy.2019.113967.
Guang, C., Zhao, X., Zhang, Z., Gao, J., Li, M., 2020. Optimal design and performance enhancement of heteroazeotropic and pressure-swing coupling distillation for downstream isopropanol separation. Separ. Purif. Technol., 116836 https://doi.org/10.1016/j.seppur.2020.116836.
Hennig, M., Haase, M., 2021. Techno-economic analysis of hydrogen enhanced methanol to gasoline process from biomass-derived synthesis gas. Fuel Process. Technol. 216, 106776 https://doi.org/10.1016/j.fuproc.2021.106776.
Iaquaniello, G., Setini, S., Salladini, A., Falco, M. De, 2018. CO_2 valorisation through direct methanation of flue gas and renewable hydrogen: a technical and economic assessment. Int. J. Hydrogen Energy 43 (36), 17069–17081. https://doi.org/10.1016/j.ijhydene.2018.07.099.
Im-orb, K., Arpornwichanop, A., 2020. Process and sustainability analyses of the integrated biomass pyrolysis, gasification, and methanol synthesis process for methanol production. Energy 193, 116788. https://doi.org/10.1016/j.energy.2019.116788.
Kerdlap, P., Low, J.S.C., Ramakrishna, S., 2019. Zero waste manufacturing: a framework and review of technology, research, and implementation barriers for enabling a circular economy transition in Singapore. Resour. Conserv. Recycl. 151, 104438 https://doi.org/10.1016/j.resconrec.2019.104438.
Kharlampidi, Kh E., Nurmurodov, T. Sh, Ulitin, N.V., Tereshchenko, K.A., Miroshkin, N. P., Shiyan, D.A., Novikov, N.A., Stoyanov, O.V., Ziyatdinov, N.N., Lapteva, T.V., Khursan, S.L., 2021. Design of cumene oxidation process. Chem. Eng. Proc. Process Intensif. 161, 108314 https://doi.org/10.1016/j.cep.2021.108314.
Kiss, A.A., Pragt, J., Vos, H., Bargeman, G., de Groot, M., 2016. Novel efficient process for methanol synthesis by CO_2 hydrogenation. Chem. Eng. J. 284, 260–269. https://doi.org/10.1016/j.cej.2015.08.101.
Klemeš, J.J., Ponton, J.W., 1992. An analysis of the efficiency of neural nets application for simulation of distillation processes. Theor. Found. Chem. Eng. 26/3, 412–424 (in Russian, English translation published by Plenum Publishing Corp, NY).
Klemeš, J.J., Fan, Y.V., Jiang, P., 2020. The energy and environmental footprints of COVID-19 fighting measures – PPE, disinfection, supply chains. Energy 211, 118701. https://doi.org/10.1016/j.energy.2020.118701.
Kumar, M., Olajire Oyedun, A., Kumar, A., 2018. A review on the current status of various hydrothermal technologies on biomass feedstock. Renew. Sustain. Energy Rev. 81, 1742–1770. https://doi.org/10.1016/j.rser.2017.05.270.
Leong, Y.K., Chen, W.-H., Lee, D.-J., Chang, J.-S., 2021. Supercritical water gasification (SCWG) as a potential tool for the valorisation of phycoremediation-derived waste algal biomass for biofuel generation. J. Hazard Mater. 418, 126278 https://doi.org/10.1016/j.jhazmat.2021.126278.
Lerner, A., Brear, M.J., Lacey, J.S., Gordon, R.L., Webley, P.A., 2018. Life cycle analysis (LCA) of low emission methanol and di-methyl ether (DME) derived from natural gas. Fuel 220, 871–878. https://doi.org/10.1016/j.fuel.2018.02.066.
Li, J., Ma, X., Liu, H., Zhang, X., 2018. Life cycle assessment and economic analysis of methanol production from coke oven gas compared with coal and natural gas routes. J. Clean. Prod. 185, 299–308. https://doi.org/10.1016/j.jclepro.2018.02.100.
Liebensteiner, M., Wrienz, M., 2020. Do intermittent renewables threaten the electricity supply security? Energy Econ. 87, 104499 https://doi.org/10.1016/j.eneco.2019.104499.
Liu, Y., Li, G., Chen, Z., Shen, Y., Zhang, H., Wang, S., Qi, J., Zhu, Z., Wang, Y., Gao, J., 2020. Comprehensive analysis of environmental impacts and energy consumption of biomass-to-methanol and coal-to-methanol via life cycle assessment. Energy 204, 117961. https://doi.org/10.1016/j.energy.2020.117961.
Liu, J., Wang, D., Yu, C., Jiang, J., Guo, M., Hantoko, D., Yan, M., 2021. A two-step process for energy-efficient conversion of food waste via supercritical water gasification: process design, products analysis, and electricity evaluation. Sci. Total Environ. 752, 142331 https://doi.org/10.1016/j.scitotenv.2020.142331.
Macrì, D., Catizzone, E., Molino, A., Migliori, M., 2020. Supercritical water gasification of biomass and agro-food residues: energy assessment from modelling approach. Renew. Energy 150, 624–636. https://doi.org/10.1016/j.renene.2019.12.147.
Mantingh, J., Kiss, A.A., 2021. Enhanced process for energy efficient extraction of 1,3-butadiene from a crude C4 cut. Separ. Purif. Technol. 267, 118656 https://doi.org/10.1016/j.seppur.2021.118656.
MathWorks, 2020. MATLAB, Math. Graphics. Programming. mathworks.com/products/matlab.html. (Accessed 9 January 2021).
Naqvi, S.R., Hameed, Z., Tariq, R., Taqvi, S.A., Ali, I., Niazi, M.B.K., Noor, T., Hussain, A., Iqbal, N., Shahbaz, M., 2019. Synergistic effect on co-pyrolysis of rice husk and sewage sludge by thermal behavior, kinetics, thermodynamic parameters and artificial neural network. Waste Manag. 85, 131–140. https://doi.org/10.1016/j.wasman.2018.12.031.
Nguyen, T.T.H., Yamaki, T., Tanuguchi, S., Endo, A., Kataoka, S., 2021. Integrating life cycle assessment for design and optimisation of methanol production from combining methane dry reforming and partial oxidation. J. Clean. Prod. 292, 125970 https://doi.org/10.1016/j.jclepro.2021.125970.
Okolie, J.A., Nanda, S., Dalai, A.K., Kozinski, J.A., 2020. Optimisation and modeling of process parameters during hydrothermal gasification of biomass model compounds to generate hydrogen-rich gas products. Int. J. Hydrogen Energy. 45 (36), 18275–18288. https://doi.org/10.1016/j.ijhydene.2019.05.132.
Olah, G.A., 2005. Beyond oil and gas: the methanol economy. Angew. Chem. Int. Ed. 44, 2636–2639. https://doi.org/10.1002/anie.200462121.
Ozonoh, M., Oboirien, B., Daramola, M., 2020. Optimisation of process variables during torrefaction of coal/biomass/waste tyre blends: application of artificial neural network & response surface methodology. Biomass Bioenergy 143, 105808. https://doi.org/10.1016/j.biombioe.2020.105808.
Pate, R., Klise, G., Wu, B., 2011. Resource demand implications for US algae biofuels production scale-up. Appl. Energy 88, 3377–3388. https://doi.org/10.1016/j.apenergy.2011.04.023.
Pérez-Fortes, M., Schöneberger, J.C., Boulamanti, A., Tzimas, E., 2016. Methanol synthesis using captured CO_2 as raw material: techno-economic and environmental assessment. Appl. Energy 161, 718–732. https://doi.org/10.1016/j.apenergy.2015.07.067.

Ponton, J.W., Klemeš, J., 1993. Alternatives to neural networks for inferential measurement. Comput. Chem. Eng. 17 (10), 991–1000. https://doi.org/10.1016/0098-1354(93)80080-7.

Poznyak, A., Chairez, I., Poznyak, T., 2019. A survey on artificial neural networks application for identification and control in environmental engineering: biological and chemical systems with uncertain models. Annu. Rev. Contr. 48, 250–272. https://doi.org/10.1016/j.arcontrol.2019.07.003.

Qin, Z., Zhai, G., Wu, X., Yu, Y., Zhang, Z., 2016. Carbon footprint evaluation of coal-to-methanol chain with the hierarchical attribution management and life cycle assessment. Energy Convers. Manag. 124, 168–179. https://doi.org/10.1016/j.enconman.2016.07.005.

Qin, Z., Tang, Y., Zhang, Z., Ma, X., 2021. Techno-economic-environmental analysis of coal-based methanol and power poly-generation system integrated with biomass co-gasification and solar based hydrogen addition. Energy Convers. Manag. 228, 113646 https://doi.org/10.1016/j.enconman.2020.113646.

Rogers, J.N., Rosenberg, J.N., Guzman, B.J., Oh, V.H., Mimbela, L.E., Ghassemi, A., Betenbaugh, M.J., Oyler, G.A., Donohue, M.D., 2014. A critical analysis of paddlewheel driven raceway ponds for algal biofuel production at commercial scales. Algal Res. 4, 76–88. https://doi.org/10.1016/j.algal.2013.11.007.

Song, C., Liu, Q., Qi, Y., Chen, G., Song, Y., Kansha, Y., Kitamura, Y., 2019. Absorption-microalgae hybrid CO2 capture and biotransformation strategy—a review. Int. J. Greenhouse Gas Control 88, 109–117. https://doi.org/10.1016/j.ijggc.2019.06.002.

Stevens, K.A., Carroll, D.A., 2020. A comparison of different carbon taxes on utilisation of natural gas. Energy Clim. Change 1, 100005. https://doi.org/10.1016/j.egycc.2020.100005.

Su, W., Cai, C., Liu, P., Lin, W., Liang, B., Zhang, H., Ma, Z., Ma, H., Xing, Y., Liu, W., 2020. Supercritical water gasification of food waste: effect of parameters on hydrogen production. Int. J. Hydrogen Energy 45, 14744–14755. https://doi.org/10.1016/j.ijhydene.2020.03.190.

Sustainability, PRé, 2020. SimaPro Life Cycle Assessment Software. presustainability.com/solutions/tools/simapro. (Accessed 9 January 2021).

Tai, X.Y., Zhang, H., Niu, Z., Christie, S.D., Xuan, J., 2020. The future of sustainable chemistry and process: convergence of artificial intelligence, data and hardware. Energy and AI 2, 100036. https://doi.org/10.1016/j.egyai.2020.100036.

Wang, C., Jin, H., Peng, P., Chen, J., 2019. Thermodynamics and LCA analysis of biomass supercritical water gasification system using external recycle of liquid residual. Renew. Energy 141, 1117–1126. https://doi.org/10.1016/j.renene.2019.03.129.

Wei, N., Xu, D., Hao, B., Guo, S., Guo, Y., Wang, S., 2021. Chemical reactions of organic compounds in supercritical water gasification and oxidation. Water Res. 190, 116634 https://doi.org/10.1016/j.watres.2020.116634.

Wu, B., Lin, R., O'Shea, R., Deng, C., Rajendran, K., Murphy, J.D., 2021a. Production of advanced fuels through integration of biological, thermo-chemical and power to gas technologies in a circular cascading bio-based system. Renew. Sustain. Energy Rev. 135, 110371 https://doi.org/10.1016/j.rser.2020.110371.

Wu, W., Pai, C.-T., Viswanathan, K., Chang, J.-S., 2021b. Comparative life cycle assessment and economic analysis of methanol/hydrogen production processes for fuel cell vehicles. J. Clean. Prod. 300, 126959 https://doi.org/10.1016/j.jclepro.2021.126959.

Yadav, P., Athanassiadis, D., Yacout, D.M., Tysklind, M., Upadhyayula, V.K., 2020. Environmental impact and environmental cost assessment of methanol production from wood biomass. Environ. Pollut. 265, 114990 https://doi.org/10.1016/j.envpol.2020.114990.

Yang, S., Li, Baoxia, Jingwei, Z., Ranjith K, K., 2018. Biomass-to-Methanol by dual-stage entrained flow gasification: Design and techno-economic analysis based on system modeling. J. Clean. Prod. 205, 364–374. https://doi.org/10.1016/j.jclepro.2018.09.043.

Ye, Z., Kim, M.K., 2018. Predicting electricity consumption in a building using an optimised backpropagation and Levenberg–Marquardt backpropagation neural network: case study of a shopping mall in China. Sustain. Cities Soc. 42, 176–183. https://doi.org/10.1016/j.scs.2018.05.050.

Yukananto, R., Pozarlik, A.K., Brem, G., 2018. Computational fluid dynamic model for glycerol gasification in supercritical water in a tee junction shaped cylindrical reactor. J. Supercrit. Fluids 133 (Part 1), 330–342. https://doi.org/10.1016/j.supflu.2017.11.001.

Zhang, H., Desideri, U., 2020. Techno-economic optimisation of power-to-methanol with co-electrolysis of CO_2 and H_2O in solid-oxide electrolysers. Energy 199, 117498. https://doi.org/10.1016/j.energy.2020.117498.

Zhang, D., Duan, R., Li, H., Yang, Q., Zhou, H., 2020. Optimal design, thermodynamic, cost and CO_2 emission analyses of coal-to-methanol process integrated with chemical looping air separation and hydrogen technology. Energy 203, 117876. https://doi.org/10.1016/j.energy.2020.117876.

Zhu, L., Hu, T., Li, S., Nugroho, Y.K., Li, B., Cao, J., Show, P.L., Hiltunen, E., 2020. Effects of operating parameters on algae *Chlorella vulgaris* biomass harvesting and lipid extraction using metal sulfates as flocculants. Biomass Bioenergy 132, 105433. https://doi.org/10.1016/j.biombioe.2019.105433.